Schweizerische Eidgenossenschaft
Confédération suisse
Confederazione Svizzera
Confederaziun svizra

Federal Department of the Environment, Transport, Energy and Communications DETEC

**Swiss Federal Office of Energy SFOE**
Energy Research and Cleantech

**Final report**

# SIRIUS

## Swiss pilot line for aesthetic and ultimate power PV modules

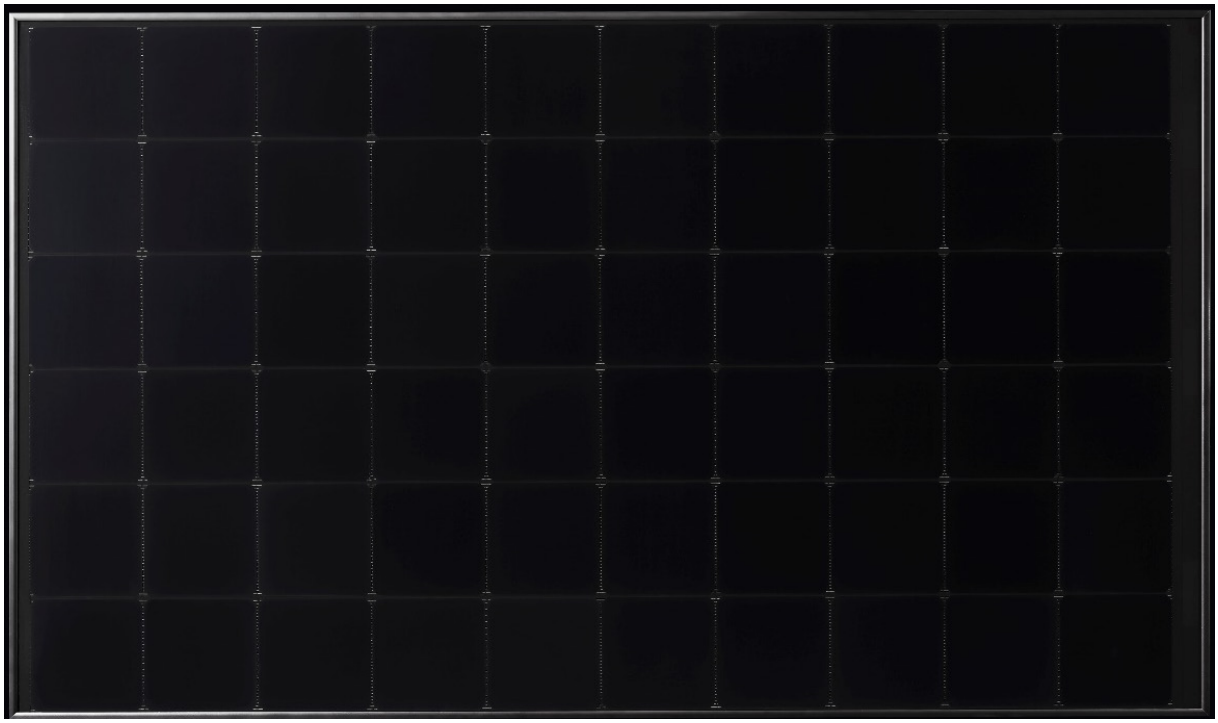

Source: ©Meyer Burger 2022

**Date:** 10 April 2023

**Location:** Bern

**Publisher:**
Swiss Federal Office of Energy SFOE
Energy Research and Cleantech
CH-3003 Bern
www.bfe.admin.ch

**Subsidy recipients:**
Meyer Burger Research
Rouges terres 61
CH-2068 Hauterive

Meyer Burger (Switzerland) AG
Schorenstrasse 39, 3645 Gwatt (Thun)
www.meyerburger.com

PASAN
Rue Jaquet-Droz 8
CH-2000 Neuchâtel
www.meyerburger.com

CSEM
Rue Jaquet-Droz 1
CH-2002 Neuchâtel
www.csem.ch

**Authors:**
Damien Lachenal, MBR, damien.lachenal@meyerburger.com
Boris Legradic, MBR, boris.legradic@meyerburger.com
Loris Barraud, MBR, loris.barraud@meyerburger.com
Jonathan Champliaud, CSEM, jonathan.champliaud@csem.ch
Jun Zhao, CSEM, Jun.Zhao@csem.ch
Rainer Grischke, MB-AG, rainer.grischke@meyerburger.com
Derk Baetzner, MBR, derk.baetzner@meyerburger.com

**SFOE project coordinators:**
Stefan Oberholzer, stefan.oberholzer@bfe.admin.ch
Karin Soederstroem, karin.soederstroem@bfe.admin.ch

**SFOE contract number:** SI/502230-01

**The authors bear the entire responsibility for the content of this report and for the conclusions drawn therefrom.**

# Zusammenfassung

Das SIRIUS Pilotprojekt, welches von den Projektpartner Meyer Burger Research, Meyer Burger Switzerland, PASAN und CSEM durchgeführt wird, hat zum Ziel, die neuartige, in der Schweiz entwickelte Rückseitenkontakt-Hocheffizienz-Solarzellentechnologie auf eine vorindustrielle Stufe zu heben, bevor diese anschließend in eine GW-Massenproduktion in der Schweiz und Europa überführt wird. Diese neue Technologie, mit der bereits unabhängig zertifiziert Wirkungsgrade von 25.4 % im Labor erreicht wurden, hat den Vorteil eines vergleichsweise einfachen Herstellungsverfahrens mit lediglich 10 Prozessschritten. Als Resultat einer 7 Jahre andauernden, gemeinsamen Entwicklung von Meyer Burger Research und CSEM entstand eine innovative Zellstruktur als Herz dieser Technologie, welche sowohl in Ihrer Struktur als auch in ihren Prozessschritten mittlerweile durch mehrere Patente geschützt ist.

Am Ende des Projekts wurden mehrere Ziele erreicht, die die Schlüsselelemente der zukünftigen Industrialisierung validierten, von der Installation einer halbautomatisierten Pilotproduktionslinie bis hin zur Produktion der neuesten Modulgeneration.. Es wurden spezifische Ziele erreicht, wie z. B. eine außergewöhnliche Modullebensdauer von über 30 Jahren, ein sehr geringer Silberverbrauch zur Metallisierung von lediglich 2,4 mg/Watt, was niedrige Herstellungskosten ermöglicht. Eine Modulleistung von 394 W (entspricht 430 W bei der aktuellen grösseren Wafer- und Modulgrösse auf M10 Format) zeigt eine verbesserte Energieausbeute von bis zu 6 % im Vergleich zur heute von Meyer Burger verkauften Heterojunction-Technologie. Schliesslich zeigten die Freilandmessungen, dass der beste im Rahmen des Sirius-Projekts hergestellte Modulprototyp mit den besten auf dem Markt erhältlichen IBC-Modulen mithalten kann.

# Résumé

Le projet pilote SIRIUS, comprenant Meyer Burger Research, Meyer Burger Switzerland, Pasan et le CSEM, a pour objectif la pré-industrialisation de la nouvelle technologie à très haut rendement de cellules solaires photovoltaïque à contacts arrières avant sa mise en production à l'échelle du gigawatt. Cette nouvelle technologie, qui a déjà démontré des efficacités de 25.4 % à l'échelle du laboratoire, a l'avantage d'une construction simple, en ne nécessitant que 10 étapes de fabrication. Cette structure innovante, protégée par plusieurs brevets, est le fruit de 7 années de co-développement entre le CSEM et Meyer Burger Research.

À la fin du projet, plusieurs objectifs ont été atteints, validant les éléments clés de la future industrialisation, depuis l'installation d'une ligne de production pilote semi-automatisée jusqu'à la production de la dernière génération de modules. Des objectifs spécifiques ont été atteints, tels qu'une fiabilité exceptionnelle de plus de 30 ans ainsi qu'une très faible consommation d'argent jusqu'à 2,4 mg/Watt permettant de faibles coûts de fabrication. Notamment, une performance de 394 W (équivalente à 430 W avec la taille actuelle plus grande des plaquettes et des modules au format M10) a démontré une amélioration du rendement énergétique jusqu'à 6 % par rapport à la technologie à hétérojonction vendue actuellement par Meyer Burger. Enfin, la surveillance extérieure a démontré que le meilleur prototype de module produit dans le cadre du projet Sirius est à la hauteur des meilleurs modules IBC disponibles sur le marché.

# Summary

The SIRIUS pilot project, involving Meyer Burger Research, Meyer Burger Switzerland, Pasan and CSEM, aims to pre-industrialise the new high-efficiency back-contact photovoltaic solar cell technology before moving into gigawatt-scale production. This new technology, which has already demonstrated efficiencies of 25.4% on a laboratory scale, has the advantage of simple construction, requiring only 10 manufacturing steps. This innovative structure, protected by several patents, is the result of 7 years of co-development between the CSEM and Meyer Burger Research.

By the end of the project, several objectives have been achieved validating the key elements of the future industrialisation, from the installation of a semi-automated pilot production line to the production of the latest generation of modules. Specific targets were achieved, such as an exceptional reliability beyond 30 years and a very low consumption of silver material down to 2.4 mg/Watt enabling low manufacturing costs. Noticeably, a module performance of 394 W (equivalent to 430 W with the current larger wafer and module on M10 size) demonstrated an improved energy yield up to 6% in comparison to the Heterojunction technology sold by Meyer Burger nowadays. Finally, the outdoor monitoring demonstrated that the best module prototype produced during the Sirius project is on par with the best IBC modules available on the market.

# Contents

# Abbreviations

| | |
|---|---|
| LIV | Light – IV measurement |
| M6 | Wafer area 274.2 $cm^2$ |
| M2 | Wafer area 244.2 $cm^2$ |
| HM6 | Half M6 |
| HM2 | Half M2 |
| SWCT® | Smart Wire Contacting Technology |
| CoO | Cost of Ownership |
| LCOE | Levelized Cost of Electricity |
| IBC | Inter digitated Back contacted solar cell |
| Tunnel-IBC | IBC solar cell featuring tunnel silicon junctions. |
| PECVD | Plasma Enhanced Chemical Vapor Deposition |
| BOM | Bill of Material |
| EL | Electroluminescence |
| PL | Photoluminescence |
| TC | Thermal Cycling |
| PTC | Powered Thermo-cycling |
| DH | Damp Heat |
| HF | Humidity Freeze |
| GBS | Glass Back Sheet (Module) |
| GG | Glass Glass (Module) |
| TCO | Transparent conductive oxide |

# 1 Introduction

## 1.1 Background information and current situation

Four years ago, Meyer Burger Technology announced a new strategy with a 180° turn from a worldwide and recognized equipment manufacturer of PV machines to a global producer of Heterojunction (HJT) solar cells and modules in Europe, with a first installation in Germany of 400 MW of annual production capacity in 2021 followed by currently the ramp-up of 1.4 GW until 2023. Continuous extension plan to multi gigawatt was foreseen until 2027. The new strategy comes from the difficulties faced in the recent years, as a pure equipment supplier, to make a substantial profit with the innovative high performance Silicon Heterojunction (HJT) technology, even though the technology was successfully proven with several customers (REC, ENEL, HEVEL). While a vertically integrated producer of cells and modules benefits from the added value by selling the final product, the equipment supplier meets strong difficulties to cover its R&D expenses in machines prototypes, processes development and globally technology development due to the sole pressure on the equipment price. The new strategy aimed to place Meyer Burger in a more profitable situation and to benefit from the continuous and rising interest in PV modules made in Europe.

Unfortunately, the PV market turned completely in 2023, with an overcapacity from China leading to a strong reduction of the photovoltaic spot price. Currently, with a spot price in the range of ~10-14 $cts/Wp (spot price for TopCon/HJT technologies), meaning a module costs about 60-70 $, the global market is in a new era and all the PV industry is under a strong pressure.

Recently, Longi, one of the bigger producer of PV panels worldwide, reported that the current situation is not economically sustainable in long term, even in China. Most probably, a general market consolidation will happen in 2024-2025 until the PV module stock starts to reduce. As a reminder, the PV module oversupply in Europe stands at ~65 GW by end of 2023 while the installation was reaching about 60 GW. With basically 1-year stock in European warehouses, the collapse of the PV spot price has triggered a cascade of factory closures in Europe, including Norwegian Crystal (Norway), REC Solar (Norway), Exasun (Netherlands), Energetic Industry (Austria) and unfortunately the biggest module factory from Meyer Burger (Module manufacturing site in Freiberg, Germany) [1].

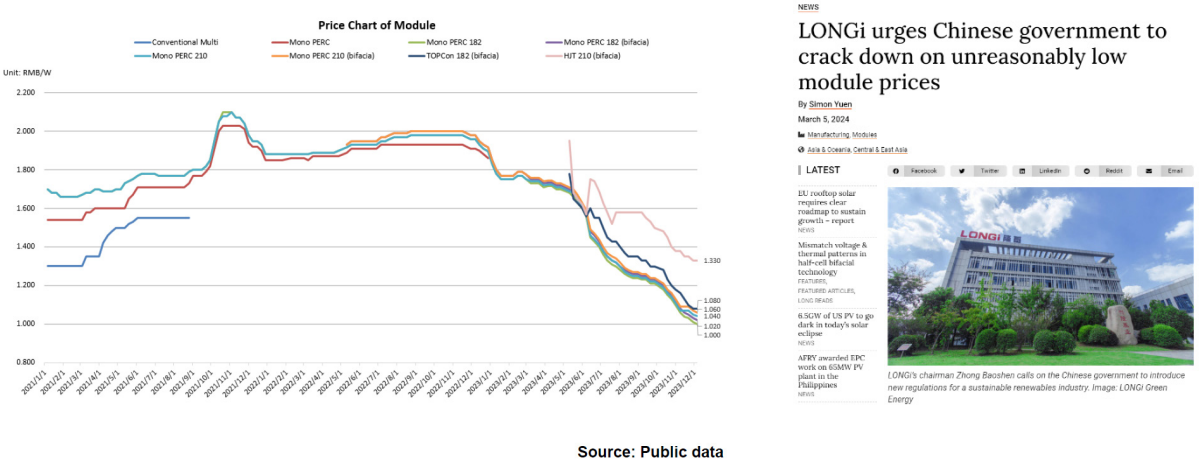


**Source: Public data**

Figure 1: PV spot price trend (RMB/Wp) and Longi's message about the PV situation in China (source PV-tech, march 2024)

Solarworld and Heckert, both located in Germany, are also considering stopping their activities in Europe [2] without state support, while Norsun temporarily suspended production of wafer in Europe.

State funds in China (94$Billion in 2023) have been used since years to enable the domination of PV production, exceeding now 609GW cumulative capacity [3,4]. In contrary to Europe where the Net-Zero Insurance Alliance law is still not finalized by the EU parliament, after the inflation reduction act in USA and Production linked incentive in India, Australia announced a similar state fund program to support the local production of PV panels and reduce the too high dependency from China.

In this difficult context, the SIRIUS project aims still at maintaining a technological edge for Meyer Burger's PV cells and modules in the coming decade, positioning durably Meyer Burger's products in the high performance – high quality segment at competitive costs, with high market shares targeted. Nowadays, two new Meyer Burger factories, one in Colorado for the cells manufacturing and one in Arizona for the module manufacturing, are under construction and will start to produce HJT modules in 2024 with off-take agreements of ~ 5.4 GW for the US market (see Fig. 2). The PV market is still in a double-digit growing phase, and Meyer Burger EDBITA is still expected to achieve 250 MCHF in mid-term. Besides the manufacturing of the HJT and the next-generation interdigitated back-contacted (IBC) cell and module technologies from the SIRIUS project, Meyer Burger potentially plans to develop a licensing business model with external companies to upscale more rapidly at lower cost its cutting-edge technology. As shown in Fig. 3, the solar deployment continues in US, with a future predominance on utilities scale products in comparison to Europe where the residential market prevails.

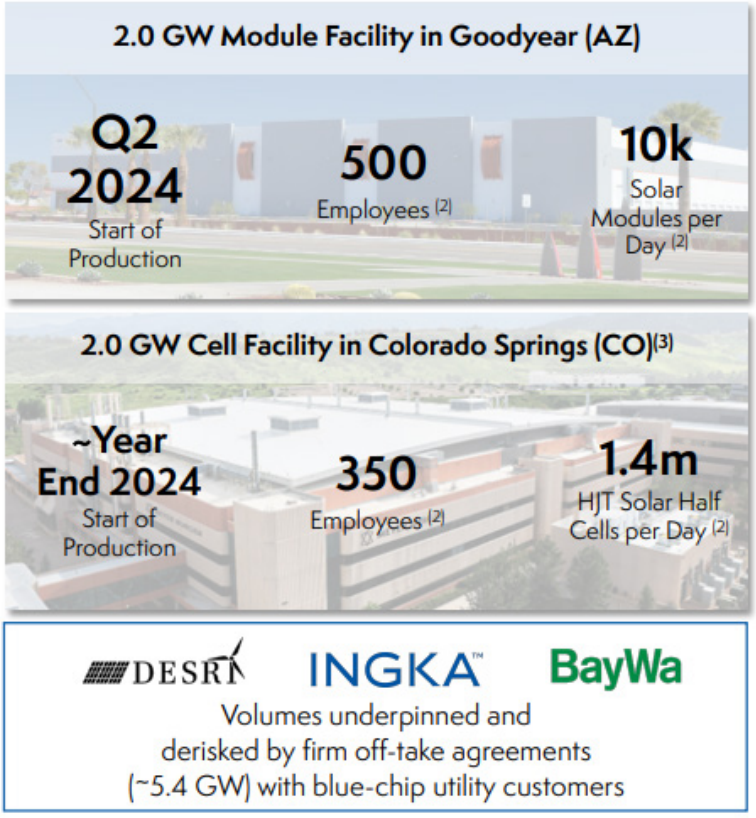


Figure 2: Key numbers of the new facilities from Meyer Burger in USA.

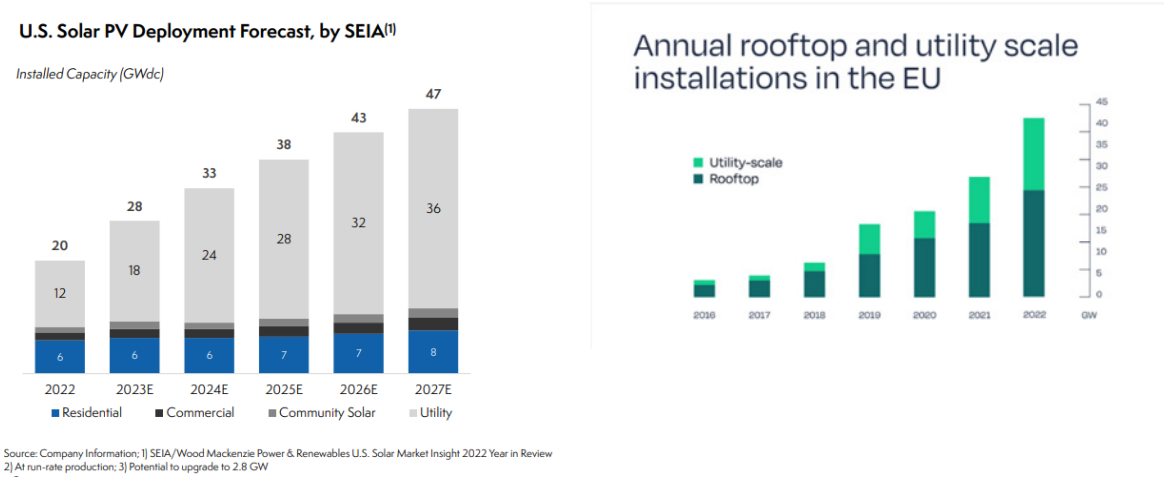


Figure 3: Difference between US (left) and Europe PV market share (right) (past, current and future).

The Meyer Burger production is focused on Meyer Burger HJT and SmartWire technologies. These production technologies were successfully developed in 2013-2016 with the support of the InnoSuisse project “Swiss-Inno-HJT”, enabling the successful sales of equipment in recent years, and being at the heart of today’s Meyer Burger strategy, with Swiss Technology produced in Europe during 3 years, and now moving to USA for the reason mentioned above.

The important challenge for Meyer Burger with this strategy is to always keep its technological edge, therefore requiring to upgrade its products in the coming years. In that frame, the objective is that the next Meyer Burger expansion plan will use a new solar cell and module technology developed between Meyer Burger Research and the CSEM during the last 7 years and only owned and mastered by these entities, namely the “tunnel-IBC” technology. This new technology features electrodes only on the rear side of the solar cells and has the potential to reach above 26% efficiency still using a single-junction, placing the tunnel-IBC technology clearly ahead from the current mainstream PERC technology and ahead from future HJT potential developments in production (forecasted to plateau respectively below 24.5 % and below 25.0 % efficiency). The key advantage of the tunnel-IBC technology is its lean process flow allowing to manufacture self-aligned silicon junctions in few process steps, consequently enabling its mass production at competitive costs. In addition, this innovative cell structure enables for cost reduction at the material level itself, as the transparent conductive oxide layer is deposited only on the rear side of tunnel-IBC devices, whereas standard HJT solar cells require transparent conductive oxides (TCO) on both their front and rear sides. Moreover, remarkably, the tunnel-IBC technology replaced ITO by ZnO (removing Indium in the bill of material of the module) and an important objective of the Sirius project is to demonstrate a copper metallization for the tunnel-IBC technology, hence completely removing silver as well.

The target is therefore to bring the ultimate PV cell solution, providing high efficiency, produced at competitive manufacturing costs, without Indium and potentially without Silver. In addition, Meyer Burger SmartWire interconnection technology SWCT®, is a key enabler of IBC solar cells implementation: it is one of the unique technologies enabling for large area IBC cells with minimum metallization usage, ease of integration and automated interconnection.

Finally yet importantly, the world record from Longi, reaching an impressive 27.3% cell efficiency recently in 2024, is based on the IBC-HJT technology. The processes are not disclosed, but it highlights that the combination of the rear IBC cell architecture together with the HJT processes enable reaching extremely high efficiencies on a single junction device. The tunnel-IBC concept brings the final advantage of a simple and lean process flow.

## 1.2 Purpose of the project

As shown in Figure 4, the previous SFOE R&D Halbion project[1] has delivered very good results with tunnel-IBC solar cells featuring efficiency up to 25.4 % independently certified on 92 $cm^2$ area. Remarkably, the same efficiency has been achieved as well on 200 $cm^2$ size (Figure 5) using the same process flow on industrial Cz n-type wafers with a thickness of 155 µm.

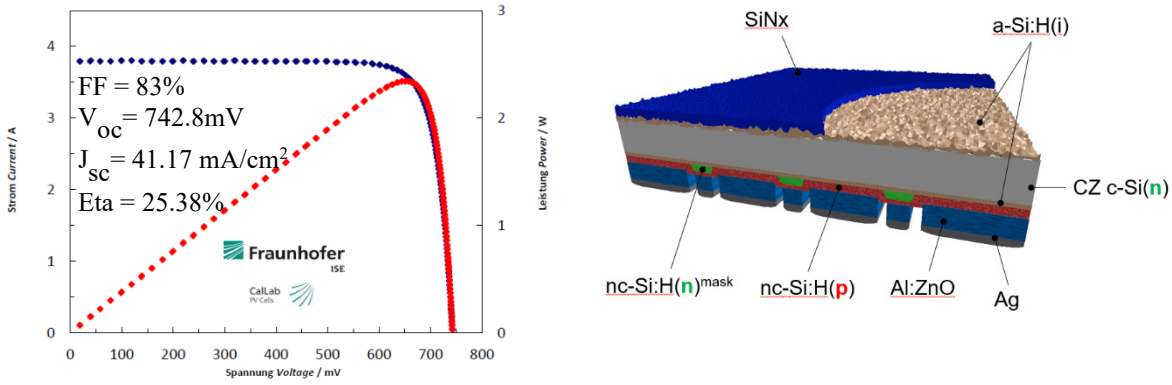


Figure 4: 25.38 % efficient tunnel-IBC device independently confirmed by the CalLab of Fraunhofer Institute of Solar Energy Systems (left) and its equivalent sketch (right).

[1] HALBION – Half bifacial back-contacted silicon heterojunction solar cells, 2019-2022, final report 10/66

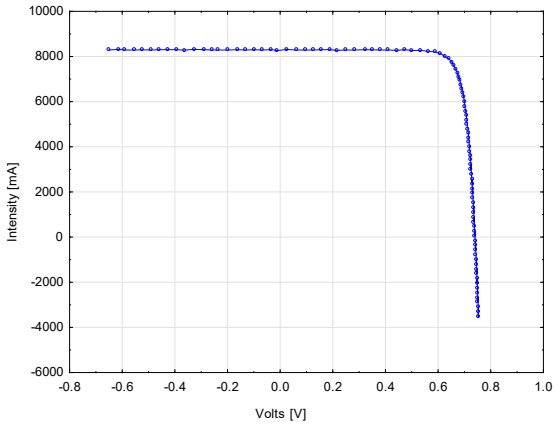


$FF = 82.68\%$

$V_{oc} = 740mV$

$J_{sc} = 41.5\ mA/cm^2$

$Eta = 25.4\%$

Figure 5: Light-IV in-house measurement of the record 200 cm$^2$, 25.4 %-efficient tunnel-IBC

These results confirmed the concept of tunnel junctions to reach high performance tunnel-IBC solar cells.

The SIRIUS project aims to develop and validate the industrialization solutions for the global tunnel-IBC and SmartWire photovoltaic technologies, before being transferred to the multi-megawatt scale at Meyer Burger production lines. SIRIUS (with TRL7 targeted at project end) is therefore the bridge between the SFOE's R&D Halbion previous project (R&D stage – TRL6 targeted) and the PILATUS MW-scale project (TRL9). The latter is currently in ramp-up phase since 2023 in Hohenstein Ernstthal, (Germany), and will serve as a basis before entering into production.

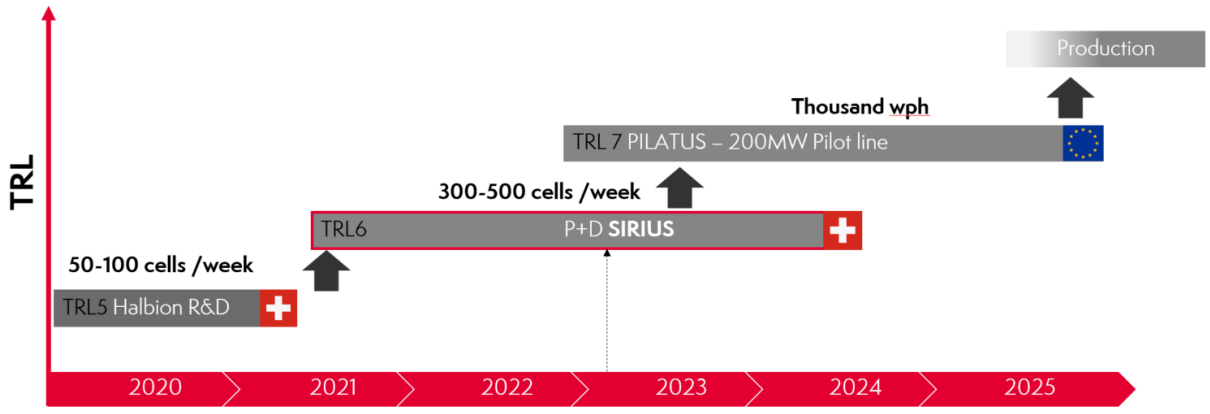


Figure 6: High-level Gant diagram of the IBC technology from R&D to mass production at Meyer Burger.

The primary goal of the SIRIUS project is the production of tunnel-IBC solar cells in a relevant environment, with a target of minimum 300 cells/week. This volume, only achievable with a semi-automated pilot line, will trigger the developments of 60-cell and 120 half-cell tunnel-IBC modules by Meyer Burger Switzerland, targeting peak power above 400 W. Behind the demonstration of the final product, the project will address the critical manufacturing steps and costs of the tunnel-IBC technology based on the current M6 wafer format. Meyer Burger Research will acquire (internally and externally) a set of new dedicated tools to process this wafer size, both at the cell and the measurement level. Meyer Burger Switzerland will develop new dedicated SWCT® tools for the IBC module manufacturing.

## 1.3 Objectives

As a reminder, the SIRIUS project objectives are illustrated in the Figure 7 below:

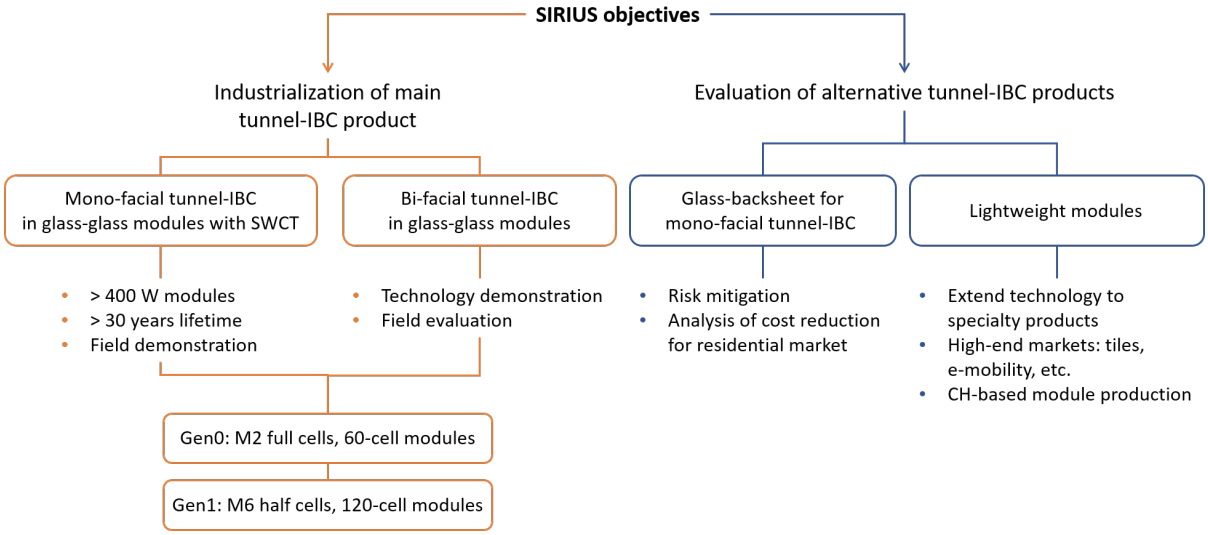


Figure 7: General objectives of the Sirius project

In order to address the defined challenges, the specific objectives of the SIRIUS project are:

- Installation of a pilot line of new machines for cells and modules manufacturing, compatible with mass production requirements.
- Demonstration of 120 half-M6 400 W module with a predicted 30-year reliability life-time.
- Installation and monitoring of 2 tunnel-IBC module technologies (16 modules in total) and benchmarking with state-of-the-art modules available on the market (Sunpower, REC, LG, PERC modules as well as Meyer Burger own HJT-SW modules).
- A significant reduction of the metallization cost, initially planned in the project to reach <150mg (but recently reviewed to reach <40mg per M6 wafer).
- Calculation of the CoO and LCOE of both module technologies developed for the residential and field PV markets.

# 2 Activities and results

The different activities and results of the Sirius project are presented below, for every work package and tasks described in the proposal:

## 2.1 Cell pilot line (WP2)

### 2.1.1 Line installation (Task 2.1)

The primary goal of the SIRIUS project is the production of tunnel-IBC solar cells in a relevant environment, with a target of minimum 300 cells/week on M6 and HM6 solar cell size. During the first year of the project, the main focus has been the conversion of the current laboratory platform to the new wafer format size, while continuing to produce solar cells on the old M2 format for the manufacturing and tests of the first generation of modules. The first year of the Sirius project included up to six internal sub-projects, each corresponding to a new machine to be installed into the laboratory either at Meyer Burger Research (Cell part) or Meyer Burger Switzerland (Module part).

At the cell level, Meyer Burger acquired two new tools and developed in-house two others tools, dedicated to the IBC technology:

- A new dedicated PECVD automation has been acquired and installed in the current PECVD system to remove the tweezers marks let by the previous manual handling of the wafers. The new automation system is able to run up to 400-450 wafer per hour with minimum marks let to the wafers. A new gripper was designed to minimize the marks let on the wafer. Automatic lifetime measurement has been integrated in the automation to monitor the passivation level of each wafer at the unloading port of the machine.
- A new PECVD prototype including the masking unit has been developed and delivered by the Meyer Burger Group. The tool is able to deposit and localize ultra-thin silicon layer to realize the tunnel junction. The system is partially automatized, with a throughput of minimum 200 wafers per hours. Delivery of specific components and materials (especially semi-conductors) was delayed by the worldwide supply chain issue, preventing to install the tool during the first year of the project, but was successfully installed in Q2 2023.

Figure 8: Picture of the new installed PECVD automation from J&R company and sketch of the new PECVD system for the tunnel junction deposition

- A new printing unit has been installed to align and print the new metallization scheme for IBC on M6 wafer size. This new versatile machine replaces the 10 years –old previous one, with a better alignment capacity. Many trials were performed to test the camera's recognition capacity on different IBC precursors. Current throughput is 200 wafer per hour. The printing line is equipped with a fully automatic loader and unloader of wafers, enabling to minimize wafers marks.
- A new set-up to measure the devices efficiency accurately has been developed internally. The measurement unit (SpotLight™) comes from the PASAN Company, while Meyer Burger Switzerland developed a dedicated automation based on a 6-axis robot to place accurately the solar cells into the measurement unit. The prototype has been installed and show a cycle time to 12s per wafer, i.e. 300 wafers per hour. The tool capacity has been extended by integrating other characterisation techniques, such as Electroluminescence and Photoluminescence measurement. This tool is a key element of the R&D line, as all the characterization methods are integrated in the same platform, enabling significant time saving and a better measurement reproducibility.

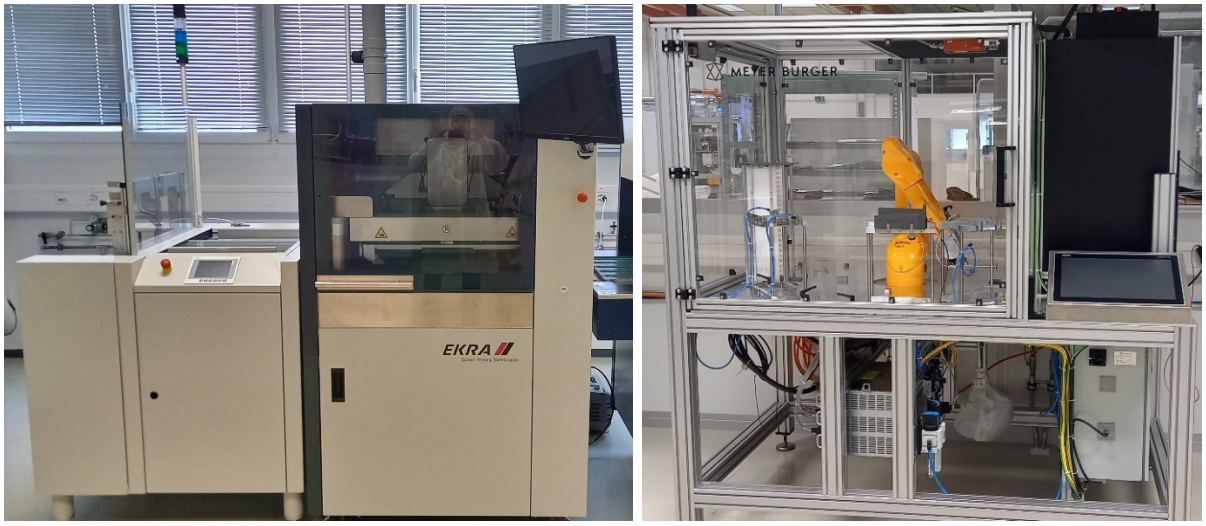


Figure 9: Pictures of the new screen printing unit (left) and the new automatized LIV system (right) dedicated to IBC measurement.

Despite the higher throughput of each new machine, some process of the IBC technology are still not equipped with automation (Wafer texturing and cleaning, PVD layers deposition, SiN deposition and laser cutting) limiting the number of solar cells to few hundred per week. The throughput gain is still significant, with a factor 5 between the previous project (Halbion, ~ 50cells/week) and SIRIUS (> 300cells/week).

### 2.1.2 Cell line ramp-up (Task 2.2)

During the ramp-up phase, the lifetime of precursors have stabilized at over 4ms after double side a-si:H(i) passivation (see Figure 10) in the current PECVD mass production platform.

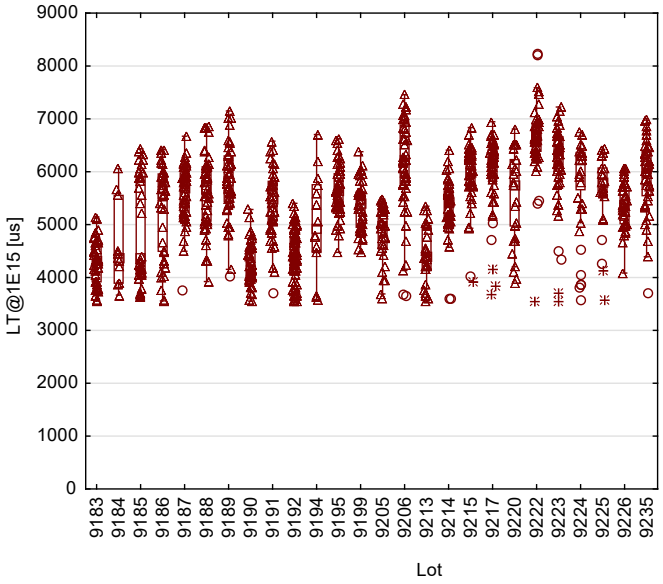


Figure 10: Stabilization of Precursor Lifetimes over 26 lots (~1200 wafers)

This improvement can be attributed primarily to the implementation of a well-calibrated automation system (see Figure 11 large view) and the optimization of various process parameters, including tray temperature, chamber conditioning, and specific plasma parameters.

The automation system, in particular, has demonstrated excellent performances and has proven its value not only in terms of enhanced handling and environmental control (e.g., prevention of scratches and dust), but also in providing greater control over tray temperature and wafer residence time. Photoluminescence (PL) images depict uniform lifetimes extending up to the edge of the samples. Figure 11 illustrates typical PL pictures of a specific lot.

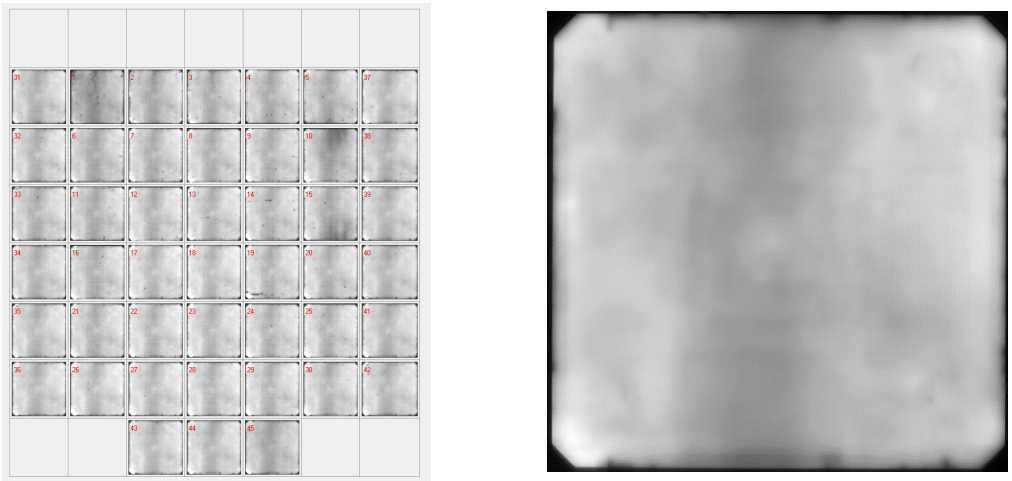

Figure 11: PL Pictures of a typical lot (left) and the superimposed PL images of the same lot (right)

Please note that the vertical stripe visible in the middle of the samples is an artifact resulting from uneven lighting in our PL system. Thanks to the fine-tuning of gripper strength and pickup parameters, the gripper marks, which were previously visible in PL images, have been eliminated. Furthermore, there have been significant improvements in emitter contact resistance understanding by using the transfer length method. By identifying the key processes contributing to contact resistance and fine-tuning relevant plasma parameters, we were able to achieve a resistance level below 40 mOhm.cm², as depicted in Figure 12. Those low values are a pre-required to reach low series resistance thus high Fill-Factor at cell level.

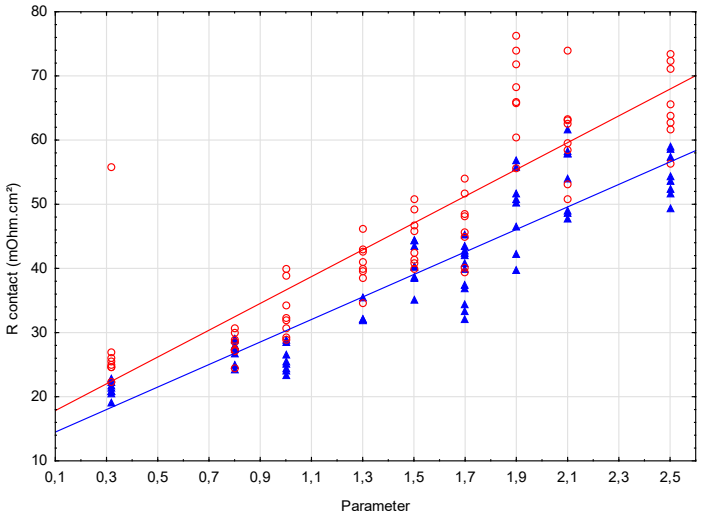


Figure 12: Emitter Contact Resistance Optimization with plasma parameter condition. Red: Emitter contact resistance samples with real IBC process flow (i.e. including vacuum break effects between layers deposition). Blue: Idem without vacuum break effect between the a-si:H(i) and uc-Si:H(p) layers.

In order to quantify the quality of contacts in solar cell technology, one has to take care about two different quantities, namely passivation and contact resistance. It has been a common methodology to measure passivation quality by either transient-Photo Conductance Decay (commonly known as Sinton measurement) or photoluminescence and contact resistance by Transfer-Length-Method (TLM). If Sinton measurement and photoluminescence are rather straight-forward and easily measurable during the process of solar cell production or on finished solar cell, transfer length method is not readily applicable and necessitate the fabrication of additional samples. Especially, for the measurement of P-type contact with TLM method, one has to use P-type crystalline wafer. This brings uncertainties and lack of measurement as TLM sample are not always simultaneously manufactured.

In order to circumvent this issue, a novel measurement of contact resistance has been developed. The idea was that the contact resistivity has to be measurable on a finished solar cell without changing the process flow and its architecture. This brings also the advantage of measuring both contact resistivity with identical PECVD patterning method. Remember that the TLM samples are manufactured with PECVD deposition made either on the entire surface of a wafer or through dedicated masks that are not the same as masks used for solar cell production.

The biggest difficulty was to find a solution for the measurement of N- and P-type contact onto N-type wafer (as P-type contact on N-type wafer is non-ohmic by nature therefore any type of TLM cannot be used). Second difficulty was the feature size. Any kind of measurement should have sub-millimeter dimensions, if one wants that it fit in P- and N-type IBC-finger. It is worth to note that such contact resistivity measurement are locally measured. Therefore, one can measure the contact resistivity on different location of the wafer surface in order to get information about the process uniformity. Moreover,

additional feature was introduced in order to measure locally the quality of the passivation through voltage measurement. This is done in a very similar way as Suns-$V_{oc}$ characterization technic is made.

Such feature is now used in solar cell development. This is bringing supplementary information on top of standard solar cell parameters. Noticeably, one can isolate both contacts independently and measure the effect of one contact polarity without interaction of the other polarity. Situation that is not met in usual solar cell parameter (namely $V_{oc}$, $J_{sc}$, FF, $R_{serie}$ and $R_{shunt}$) where such parameters always carry information of both contact polarity. This could be even more complex in monofacial cell technology as the uc-Si:H(p) layer (called puc, alternatively nuc for n-contact) deposition is made on the entire surface (N-contact area is underneath puc layer). As an example, if one is changing any properties of puc layer it may influence P- and/or N-type contact resistivity.

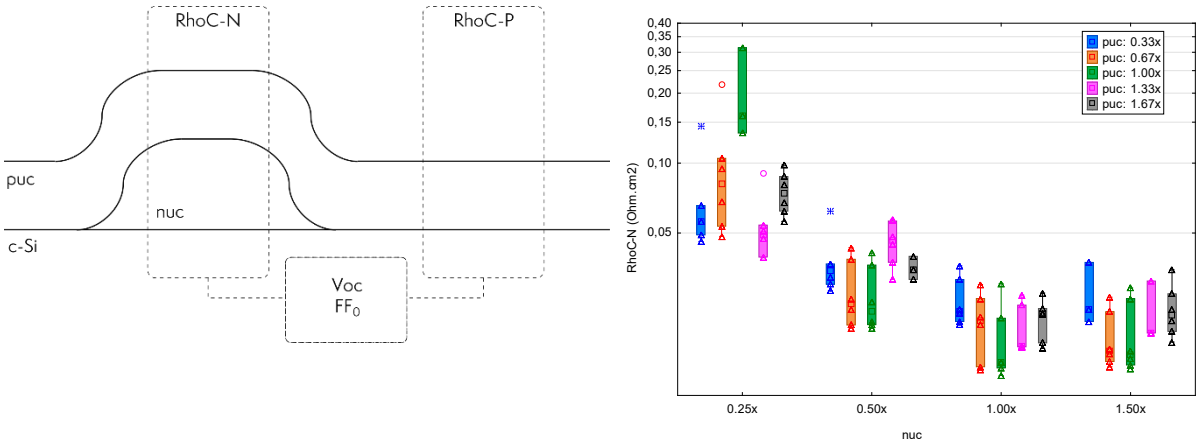


Figure 13: Sketch of back contact resistivity measurement. N-type contact resistivity (RhoC-N) is measured on location of nuc deposition through the PECVD masks. Whereas, P-contact resistivity is measured in between N-finger, where the emitter is formed. Both feature are used in order to measure the passivation quality reflected in the sketch as $V_{oc}$/FF0 (Left). Example where N-type contact resistance is measured while varying thickness of puc and nuc simultaneously (Right). Remember that N-type contact comprises both nuc and puc stacks. Therefore, one can see the influence of puc on N-type contact resistivity.

On the new PECVD platform, an excellent wafer uniformity thanks to the new masking unit has been reached as presented in Figure 14:

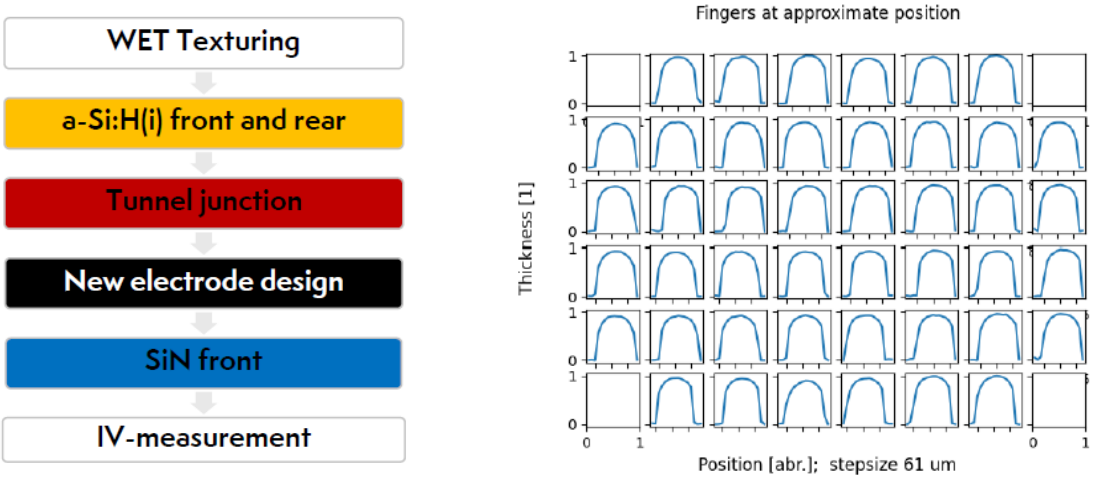


Figure 14: Tunnel IBC cell process flow (left) and thickness uniformity of the localized nuc layer over a whole wafer (right) showing a uniformity +/-3%.

This excellent uniformity of the patterned layer is combined with a silicon surface free of damage, as shown from the PL measurement below:

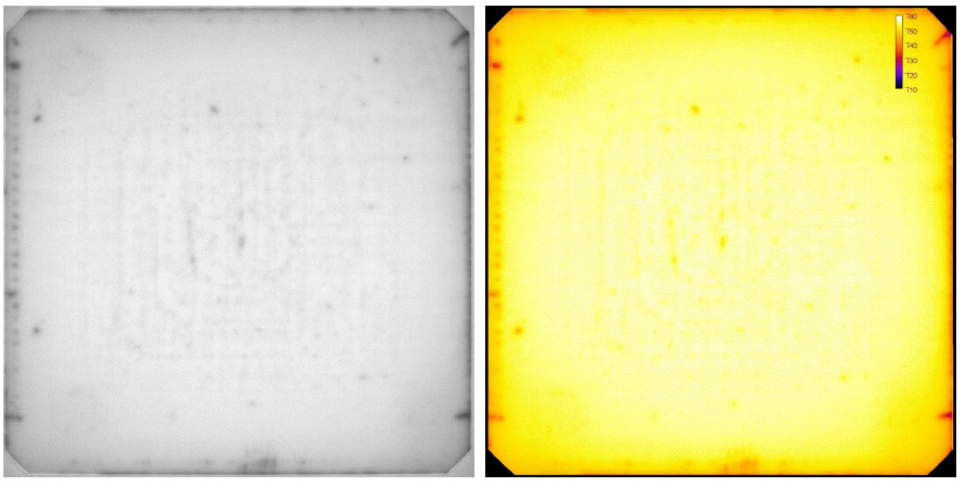

Figure 15: Photoluminescence picture (1sun) with i/nuc$^{mask}$/puc (left) and corresponding implied $V_{oc}$ (right)

At the Cell tester device (Figure 16), we developed the automated IV measurements further and added improvements to the operational capabilities of the automation. On the automation side adjustments of the paper handling greatly improve the stacking, de/re-stacking, sorting and binning reliability (previously insufficiently well-handled paper eventually led to cell breakage), i.e. ultimately we could increase tool uptime and throughput considerably. With the feedback from the module backend automation, geometrical HM6 cell control was improved so that cells with small deviations from the required standard format are sorted out at testing and will not complicate the latter stringing process anymore. Furthermore, cell dimensions are now measured and displayed directly for each cell and data is accessible via an output data file in csv format, thus allowing for correction of area related IV parameters like current density $J_{sc}$ and efficiency Eta.

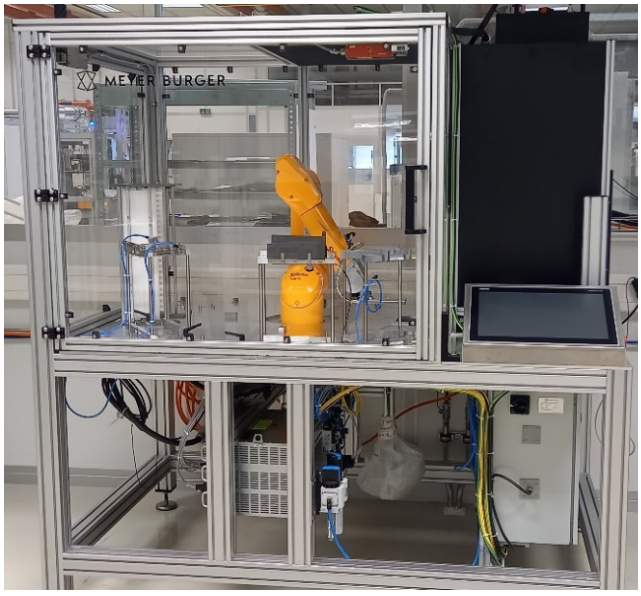


Figure 16: Picture of the developed automated IV measurement system

We further improved the automation functionality to better cater to the requirements in development. Automated batch measurements can now be easily paused and continued if required, e.g. to replenish the paper supply or exchange/remove unwanted elements in the handling unit. Paused batch measurements can be continued with minimal time interruption and greater flexibility in carrier and box loading.

For development and in-depth analysis purposes, we added a semi-manual mode that enables manual positioning and alternation of devices to be measured, combined with the powerful automation capability to trigger a whole sequence of measurements and automatically save results in our data base compatible structure for later efficient and advanced data treatment and analysis. On the cell tester side as a major scientific upgrade, we now included the capability to measure the photo luminescence (PL) of cells which is key to a new much improved level of testing productivity. With the final step of this PL-integration we have brought together characterization techniques previously carried out manually in various, individual tools into one single, automated testing unit that is capable of running entire testing sequences (i.e. multiple free assignable single measurements) with each cell or precursor, respectively. The adaptations of the PLC (Programmable Logic Controllers, coordinate the individual elements across the entire unit/tool) allow now to define up to 16 individual measurement sequences. A sequence can be either:

- 1x PL measurement (with adjustment for injection) or
- 1x EL measurement and/or 1 IV measurement.

On the automation side, 16 of those freely definable sequences can be selected for execution with every cell in deliberate order. To each measurement in a sequence a recipe, i.e. a specific parametrisation of the measurement, can be assigned, that gives great flexibility in taking different measurement on a cell determined by the chosen sequence with the included measurement recipe.

Currently, our standard characterisation contains 6 measurements for each cell triggered by 4 individual sequences:

- PL measurements, one with 1 LED illumination with a center wave length of 640nm and an injection of approx. 550W/m$^2$ and one measurement with 2 LED illumination with a center wave lengths of 640nm and 910nm, respectively, that add up to 1000W/m$^2$
- EL measurements, one at a high injection level above $I_{sc}$ and one at a low injection level of less than 10% of $I_{sc}$.
- 2 IV measurements; with and without dark IV and at slightly different sweep duration.

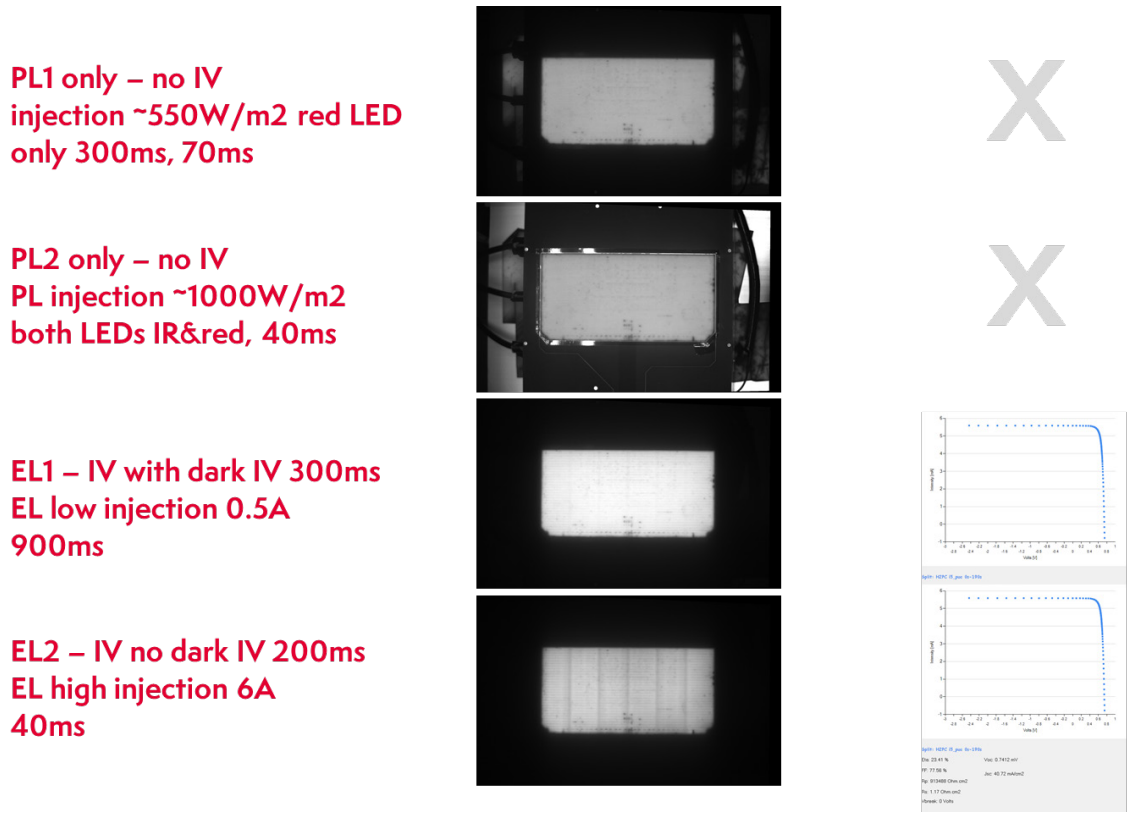


Figure 17: Overview with examples over standard measurement sequences applied on each individual HM6 cell

These six measurements which include four images of each cell enable us to literally get a much better picture of each measured cell. We have developed a script and an entirely new metrology that batch processes the raw images further, calculates meta-data from the signal of the active cell area contained in the images, e.g. average values and uniformity. Additionally, applying the newly developed metrology we further process the raw images into new images that enable us to visualise distinct cell aspects like for example the contact quality in an intuitively understandable new images.

The most accessible resulting images are quantified/calibrated maps of $V_{oc}$, series resistance $R_s$, and a normalised 'contact-map' that indicates zone of inferior contact quality in a different color. These visualisations are very helpful for a fast and effective identification of process related issues like defect generation by scratches during the deposition of the PECVD layers or process uniformities that are otherwise difficult or impossible to characterise.

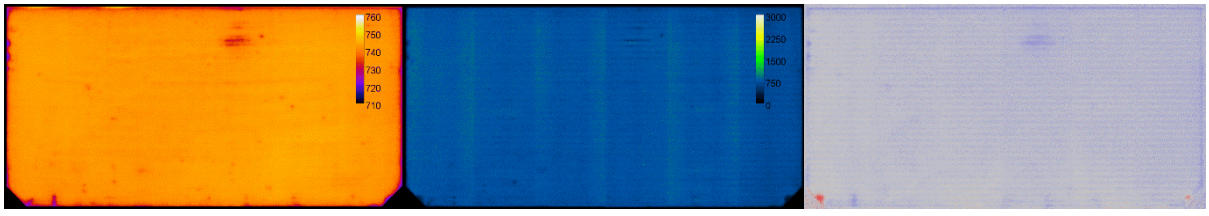


Figure 18: left, $V_{oc}$ map of a good cell scaled in mV; middle, $R_s$ map of same HM6 cell scaled in $m\Omega.cm^2$; right, uniform 'contact map'

We have been monitoring the repeatability of IV measurements and contacting. Both are of sufficient precision and accuracy for our current application. We now also understand the requirements for a reliable contacting in production that ensures precise evaluation of the cell parameters like the CE.

The repeatability of the IV measurement is the inherent property of the SpotLight tester, the reliability of contacting is due to a sufficiently precise positioning of cells onto the contact unit by the robot and vision of the automation part of the tester and the cell's electrode design together with the contacting unit that are accommodating small variations in placing. From image analysis we estimate placing variations on the PCB to be ±0.2-0.3 mm. Innovations and measures taken to improve cell contacting have been proceeded to a patent application to protect the developed IP.

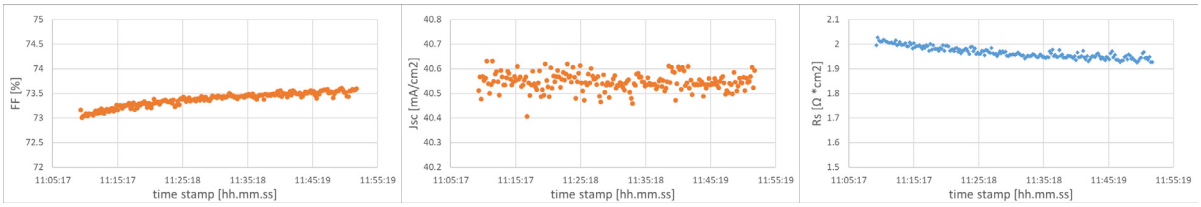


Figure 19: Positioning and measurements repeated 200 times consecutively on sample cell with 22% efficiency; left to right evolution of FF, $J_{sc}$ and $R_s$ over the testing duration. FF and $J_{sc}$ show good but not perfect precision, which is caused by variations in cell positioning. Additionally, we observe a conditioning of the cells during measurements that improve cell performance slightly, notable in an increased FF and decreased $R_s$.

With the capability to take PL measurements with the new automated tester we switched from a process control via manual PL measurements, to an automated PL control before cutting the M6 precursors into HM6 cells. This is quite effective and $V_{oc}$ maps of each cell before cutting are readily obtained from the PL images without the need to contact the precursors. This is even more interesting when we will apply the procedure on cell precursors after PECVD deposition steps, so before they even have contacts that would allow the electrical voltage measurement. We are planning to introduce that further metrology step at the time when we process wafers in the new PECVD equipment.

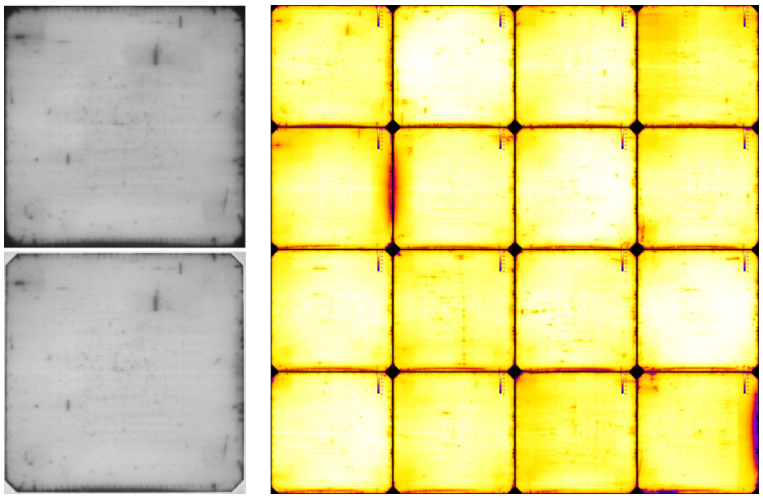

Figure 20: Example of PL measurements on full wafer cell or precursors; left: raw images at different injections, right: montage of 16 calculated $V_{oc}$ maps (scale 700-750mV)

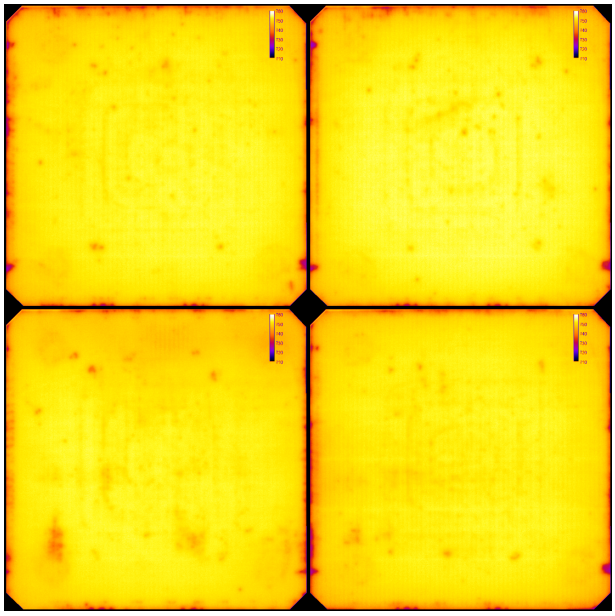

Figure 21: Example of automated PL measurements on full wafer precursors after deposition of all PECVD layers with calculated $V_{oc}$ maps (scale 710-760mV), note the higher PL signal on precursors compared to final cells indicates the even higher $V_{oc}$ potential.

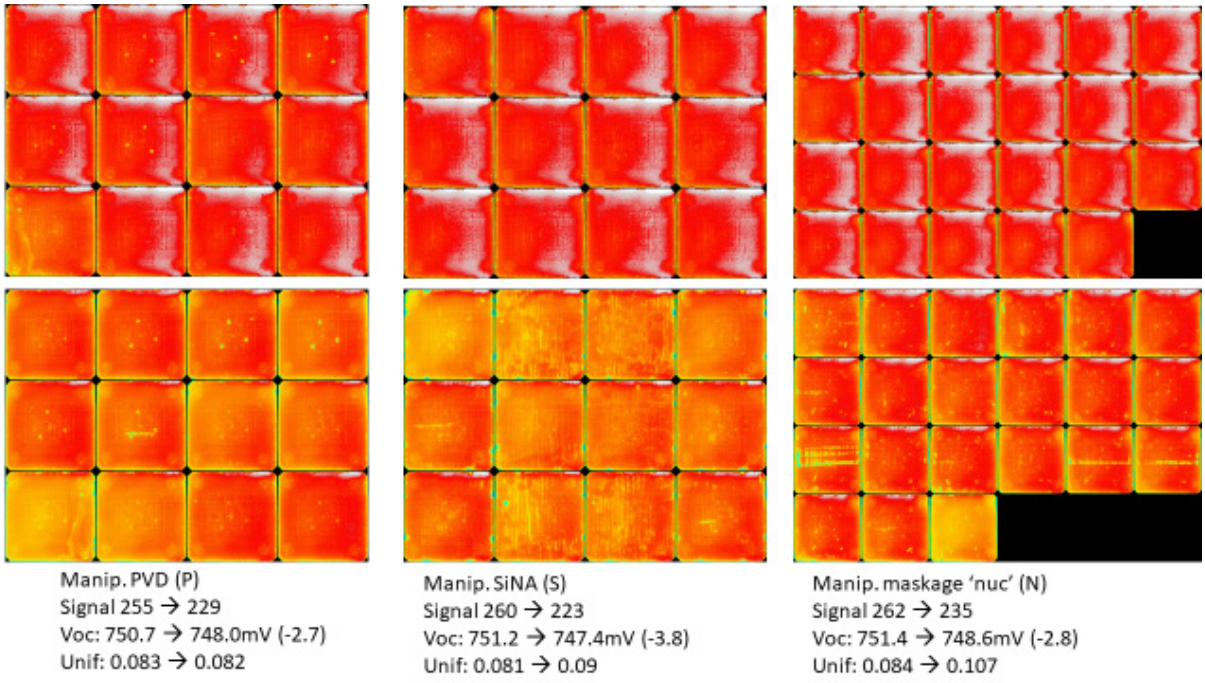


Figure 22: Example of automated PL measurements on full wafer precursors as passivated (i/i) rows on top and after manual handling rows underneath. The new methodology allows to visually identify manipulation damage as well as quantify the impact on final cell performance which enables a much more precise loss analysis across all processes.

With the automated PL characterisation on entire lots we can leverage this methodology to establish performance loss analysis like the impact of manual handling of wafers as shown in the example in Figure 22. The example above also highlights the importance of automation in processing, since it shows as in the above example a potential ($V_{oc}$) loss and by uniformity loss also a negative impact on FF with each manual handling step that can be largely or entirely avoided with a proper automated wafer handling. Thus, it also shows that (and how much) our current IBC cell processing has upward performance potential in a large scale production.

These advances in characterisation helped us to identify uniformity losses and were instrumental to overcome or minimise processing issues that severely hampered the progress in our targeted performance roadmap with the format change from M2 to M6 substrates in our pilot line. As a result, we are now able to process HM6 cells with efficiencies of well above 24 %.

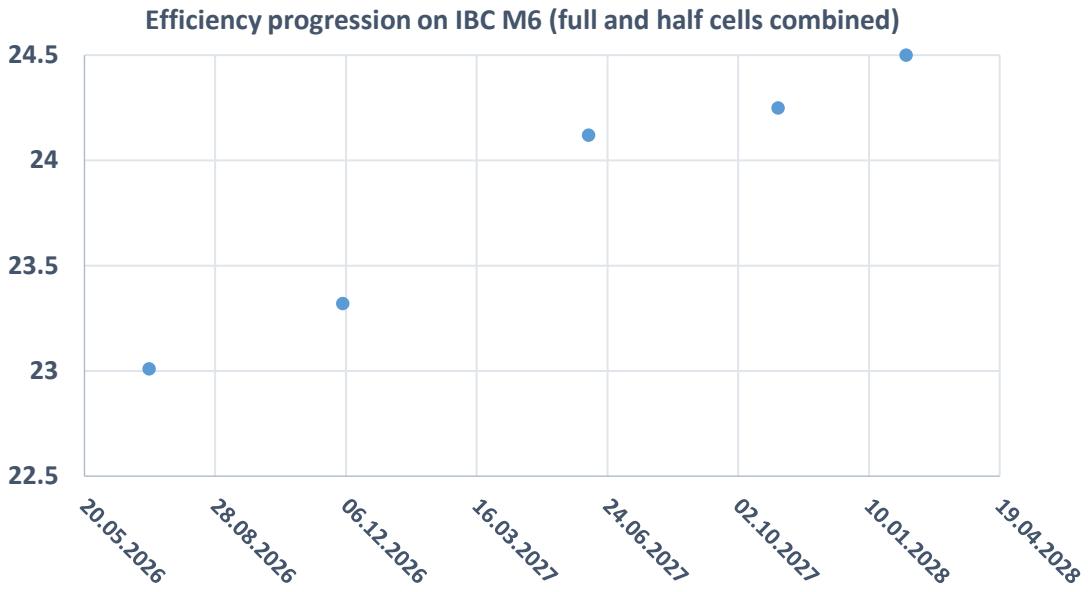


Figure 23: Champion cell efficiency progress over the project duration.

### 2.1.3 Mono-facial electrodes development (MBR, M1-M36) (Task 2.3)

The aim of this task was first to reduce the amount of silver metallization per cell, in order to enable the tunnel-IBC solar cells to be cost competitive when compared to the PERC and the future TOPCON mainstream technology and next, to optimize the cell to module power loss by optimizing the module and the cell design. The silver consumption in PV is a hot topic [5, 6] since the significant increase of PV production over the last years. Figure 24 presents the supply/demand of silver worldwide for different category of usage, and shows the importance nowadays of PV in the global demand. While the industry (without PV) has a stable consumption since 10 years (~400 Million ounces /year), the PV is the only market with a continuous growth of the demand. Since 2021, the total silver demand exceeds the supply. Alternatively, the usage and available resources is depicted on Figure 25, highlighting the strong pressure on Indium, Silver and Copper materials based on the known resources today [7-10].

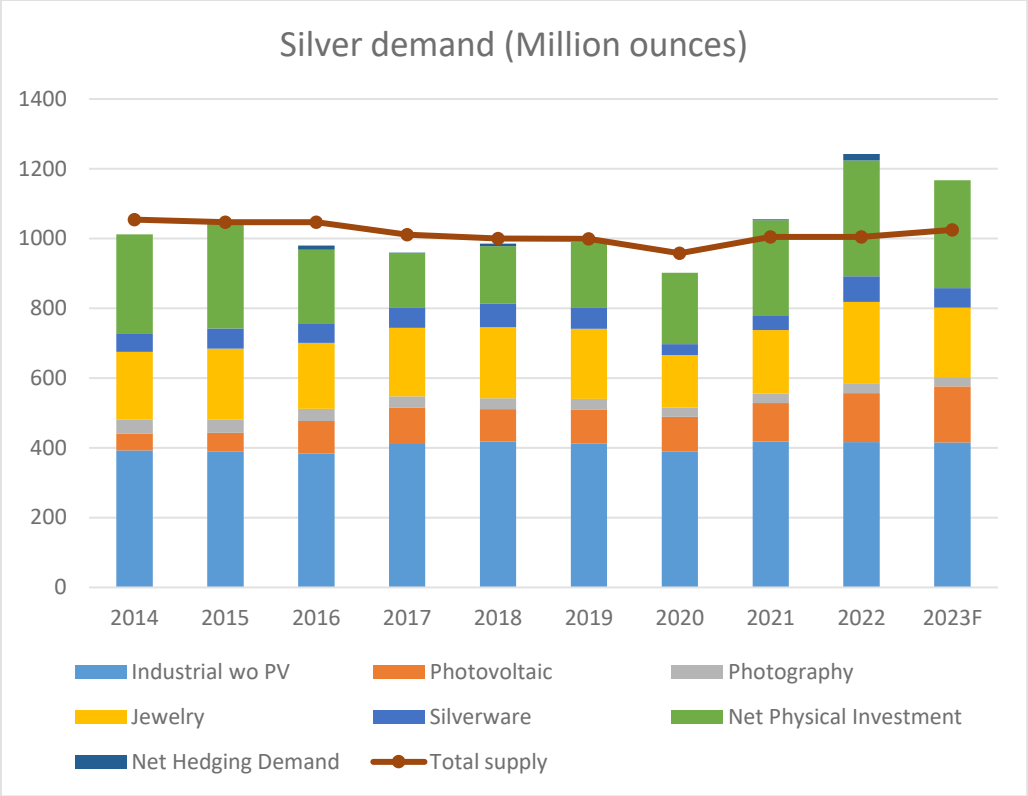


Figure 24: worldwide Silver supply/demand

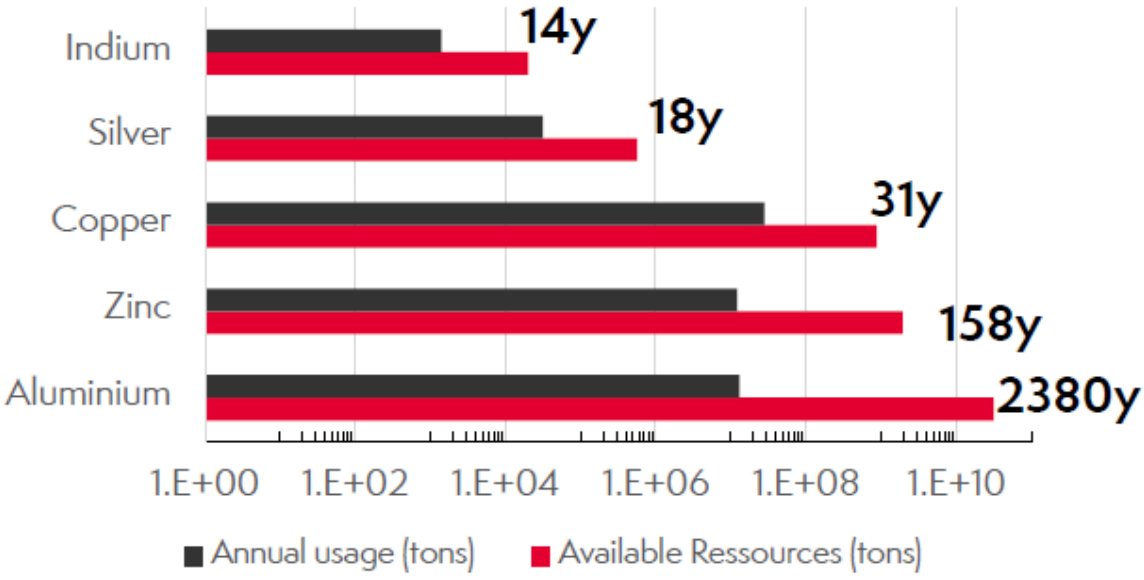


Figure 25: Resources availability for typical raw material used in solar cells.

The work on silver consumption during the first year of the project has been carried out on M2 wafer format, as M6 precursors were not ready yet. The optimization of screen printing design allowed to reduce step by step the screen printed silver paste from 150 mg to 75 mg while running contact resistivity simulation separately. We observed no difference of Fill-Factor (FF), neither cell efficiency (Eta) by reducing the silver consumption by a factor two (Figure 26).

| | Electrodes design 1 | Electrode design 2 |
|---|---|---|
| Ag consumption | 150 mg | 75 mg |
| M2 Cell Efficiency (Max/mean) | 24.1 %/23.6 % | 24.2 %/23.6 % |

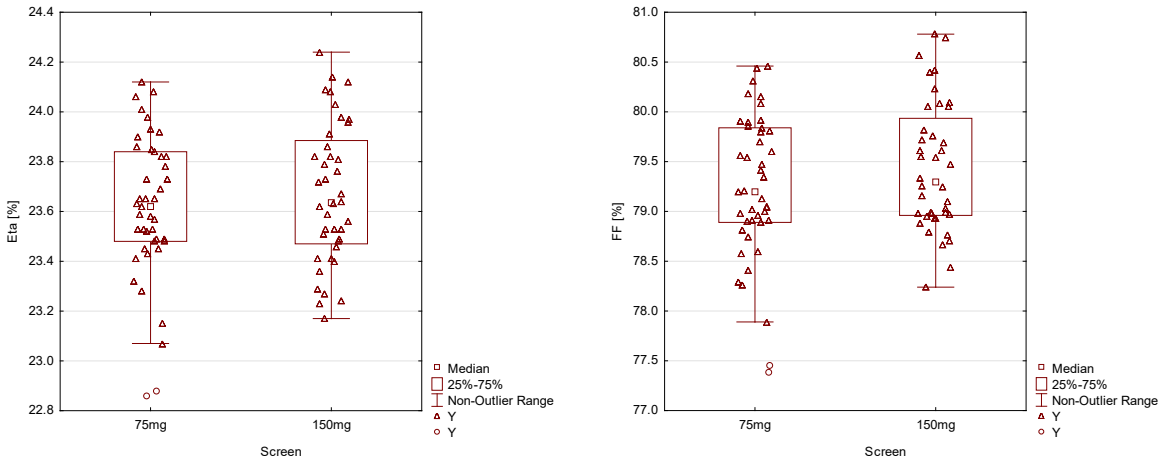


Figure 26: M2 Cell efficiency and Fill-Factor for two electrode designs featuring either 150mg or 75mg of silver.

The experimental data are confirmed by analytical simulations on Figure 27 where the Fill-Factor losses are estimated as a function of contact resistivity and silver consumption. Electrode with low silver consumption needs contact resistivity below ~ 200 µOhm.cm$^2$ to limit Fill Factor loss to an acceptable level (0.1 %).

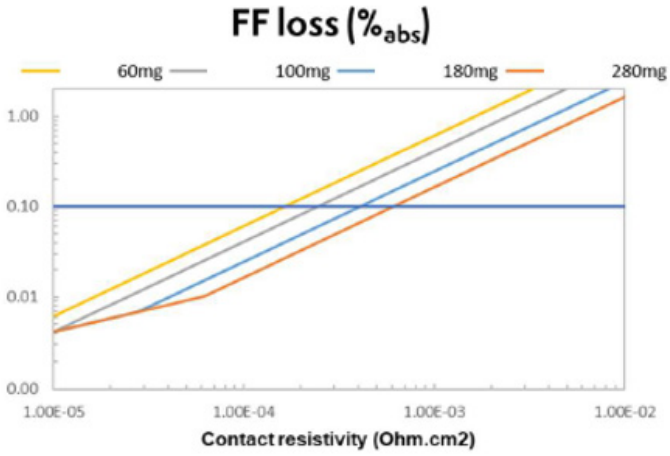


Figure 27: Simulation of Fill Factor loss as a function of contact resistivity for different silver consumption on a M2 wafer.

This good result confirms the electrical robustness of the chosen electrode design, even with low silver consumption. M2 to M6 cell format conversion impacts negatively the silver consumption (from 75 mg to 84 mg) due to the increased wafer area, but remains competitive when compared to the PERC reference (about 80 mg silver paste per M6 wafer). During the second year of the project, the implementation of Ag/Cu metallization paste and a further optimization of the electrodes design were successfully tested, allowing to further reduce step by step the net silver content to only 15.5mg per HM6 cell, i.e. an equivalent to 2.4 mg/Watt. This metric is commonly used to compare the silver consumption for the different technologies (PERC, TOPCON) with different wafer format. Figure 28 compares the silver consumption for the mainstream PV cells including the tunnel-IBC cell developed in this project and highlights the promising production cost perspective for this new technology.

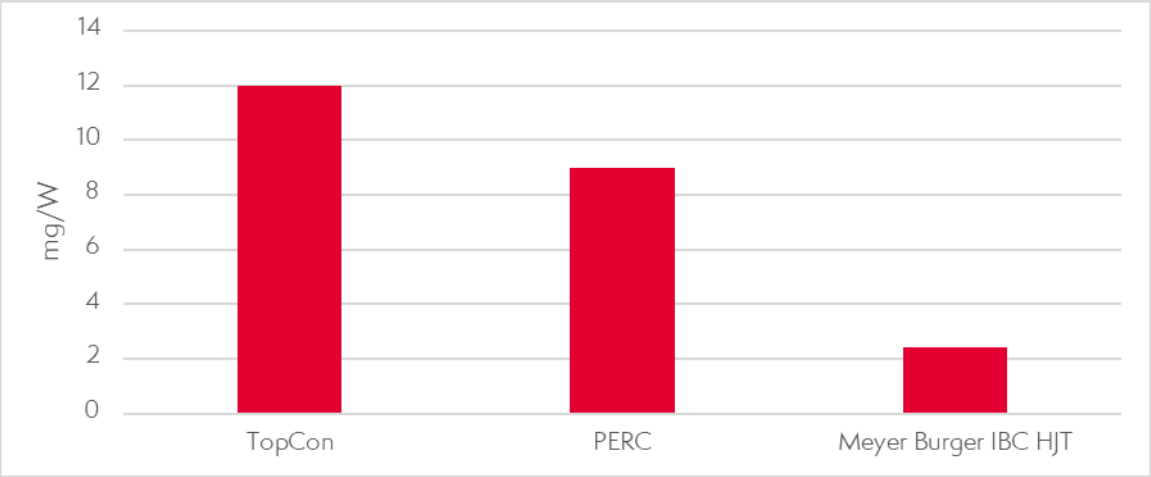


Figure 28: Average net silver consumption per technology mg/Wp [6].

During the third year of the project, one task was to adapt the process to industrial environment. To ensure high production throughput, squeegee movement speed has been raised from 50 mm/s up to 300 mm/s for all back end process steps. Thanks to different studies on the impact of screen to wafer gap, squeegee print pressure and screen physical specifications we have been able to fulfill this objective. The ratio of badly printed samples is very low and thanks to the increase of the screen-printing speed, the metal paste laydown was further reduced by up to 30 %.

Thanks to the continuous improvements and higher control of each process step, the quality of the IBC backside structuring alignment has been greatly improved. Thanks to that, the edge exclusion between backside electrodes and wafer edge has been reduced from 900 to 200 µm. As shown in Figure 29, the Laser Beam Induced Current (LBIC) signal with small edge exclusion is higher than with 900um edge exclusion. This improvement allows better collection of electrons & holes carriers generated by the light close to the wafer edge and we have measured a boost of $J_{sc}$ of about 0.3 mA/cm$^2$ thanks to this improvement.

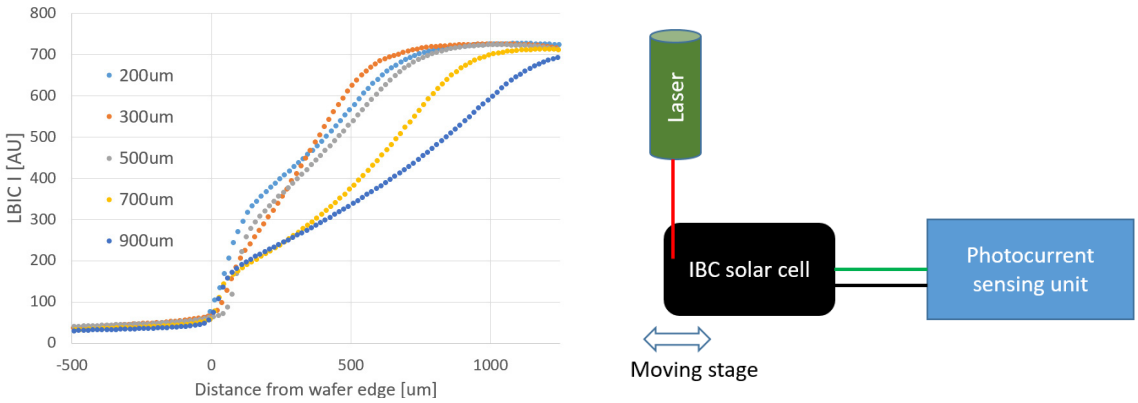


Figure 29: Laser Beam Induced Current measurement on IBC cell edge.

Along this third year of development, a large amount of test structures and characterizations was conducted with the objective to figure out key parameters that affect IBC solar cell series resistance. Series resistance limits cell electrical performances and determines its key contributors allowing us to prioritize our research to reduce their influences and therefore boost IBC cell and module performances. All these measures and data were interpreted and completed with varia simulations (Quokka, Griddler, Spice…).

Figure 30 presents the distribution of key factors that affect HM6 IBC solar cell series resistance. Cell passivation, layer thickness and properties uniformity are the main contributors of the series resistance of HM6 IBC cell. This parameter can be reduced by improving layer deposition uniformity and smoother handling of the wafer during each process steps. Indeed, at MBR, despite the automation for the i/i layers passivation presented above, many wafer transfers are still done manually and due to this fact, many scratches are observable on our finished solar cells. The second key element that makes up the IBC series resistance is the limited contact resistance on the P doped area. Despite its large area fraction on cell backside, this contact limits strongly IBC cell performances and many new research try to reduce its impact. In contrast, the N contact is good and its impact is almost negligible. Ohmic losses on the wafer and metal back electrodes present small impact on the IBC solar cell series resistance and little gain is expected by improving them.

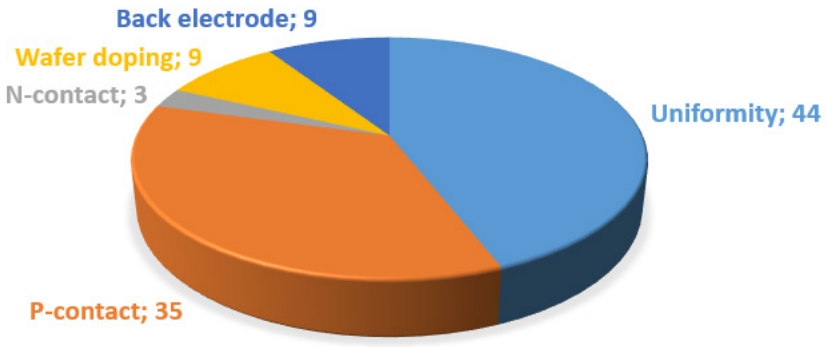


Figure 30: Main elements (%) impacting the series resistance of the tunnel HM6 IBC solar cell

### 2.1.4 Bi-facial (Bifi) electrodes development (CSEM, M1-M36) (Task 2.4)

In our 1st simulation on the AZO sheet resistivity and finger configuration, we have learned about some bottlenecks of the contact resistivity between AZO and metal fingers. This simulation provided us further ideas, how the process for the Bifi configuration be further optimized. Based on the simulation results, an experiment with splits on the AZO sheet resistivity has been done and the contact resistivity and line resistance of all AZO samples have been measured and compared with ITO. Another more transparent resin paste for improved bifaciality has been qualified and replaced the current resin paste. To reduce the amount of resin deposited and thus improve contact with the metal, the print was made in Print/Print mode (i.e. consecutives cells are printed with different resist print direction) instead of Flood/Print (i.e. all cells are printed in the same condition, the resist being put back at its initial location on the screen prior printing) mode. The finger geometries have been measured and checked for the uniformity in single and double print mode within full size M6 substrate. Due to the 2nd simulation, the impact of different bifacialities, number of fingers for n/p regions and illumination from front and rear side have been taken in account.

a) 1st 3D finite-element simulation

To validate if the concept of Bifi IBC is viable, especially regarding potential lateral transport losses. The most relevant parameters have guided on the actual M6 design. Full 3D model of IBC Bifi was established with Sentaurus TCAD. To understand the effect of AZO doping in Bifi IBC, kind of “corner cases” of two extreme $R_{sheet}$ of 3 Ω /sq and 300 Ω /sq in combination with two different pitch distances were tested in the simulation. As out coming results in Figure 31, a FF>80 % is still possible, even in case of low AZO $R_{sheet}$, owing to the lateral transport in the c-Si bulk. Smaller pitch has shown a gain of +0.5-0.8 % in FF. From the contact point of view, a clear FF loss with high $R_{sheet}$ 300 Ω /sq AZO was observed. For the device optimization, electrical and optical properties trade-off will be required.

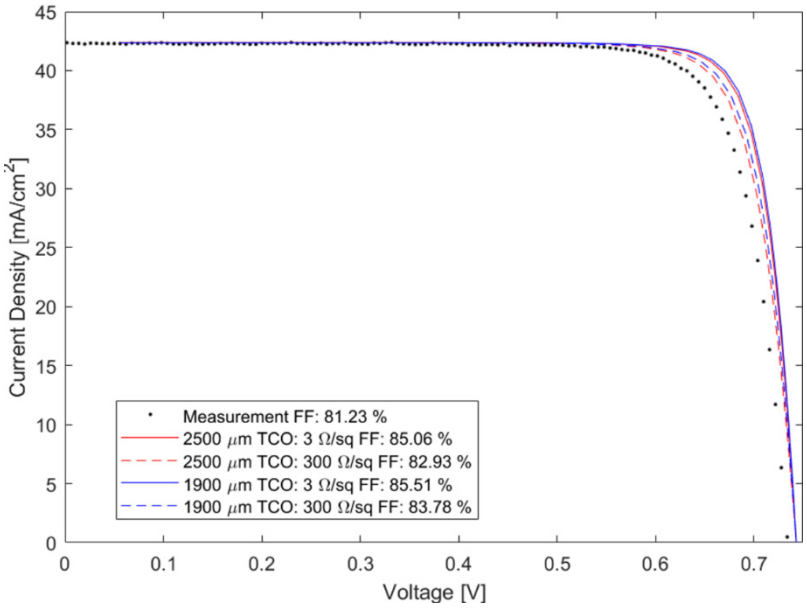


Figure 31: effect of AZO doping in IBC Bifi configuration

In the simulation for the rear grid design vs AZO doping optimization (Table 1), the numbers of fingers are not the main driver in case of low $R_{sheet}$. It enables simpler screen design and more efficient etching.

| Design | FF @ TCO 3 Ω/sq | FF @ TCO 300 Ω/sq |
|---|---|---|
| 2N/4P (old design) | 85.51 % | 83.78 % |
| 1N/2P | 85.44 % | 82.07 % |

Table 1. Optimization of rear grid design vs. AZO doping

In the simulation about the effect of reduced metal/AZO contact area in IBC Bifi, a reduced metal/AZO contact area might be a show-stopper for IBC Bifi. A contact resistance ~$10^{-3}$ Ω.cm$^2$ is probably needed, which is 10% of the level at that time.

b) AZO characterisation

To follow the trend of the 1st 3D simulation, AZO in 4 conditions from CSEM, 1 condition from MBR and 2 samples with ITO from MB production as reference were prepared for the contact resistivity and line resistance measurements. In the graph of contact resistivity, Figure 32, the contact resistivity became worse by increasing of $Ar/O_2$ ratio. Apparently, standard 10 min of curing at 210 °C seems not enough to reach the 1 mΩ.cm$^2$ with AZO. With 30 min curing condition, some AZO samples are able to reach the specification of required contact resistivity.

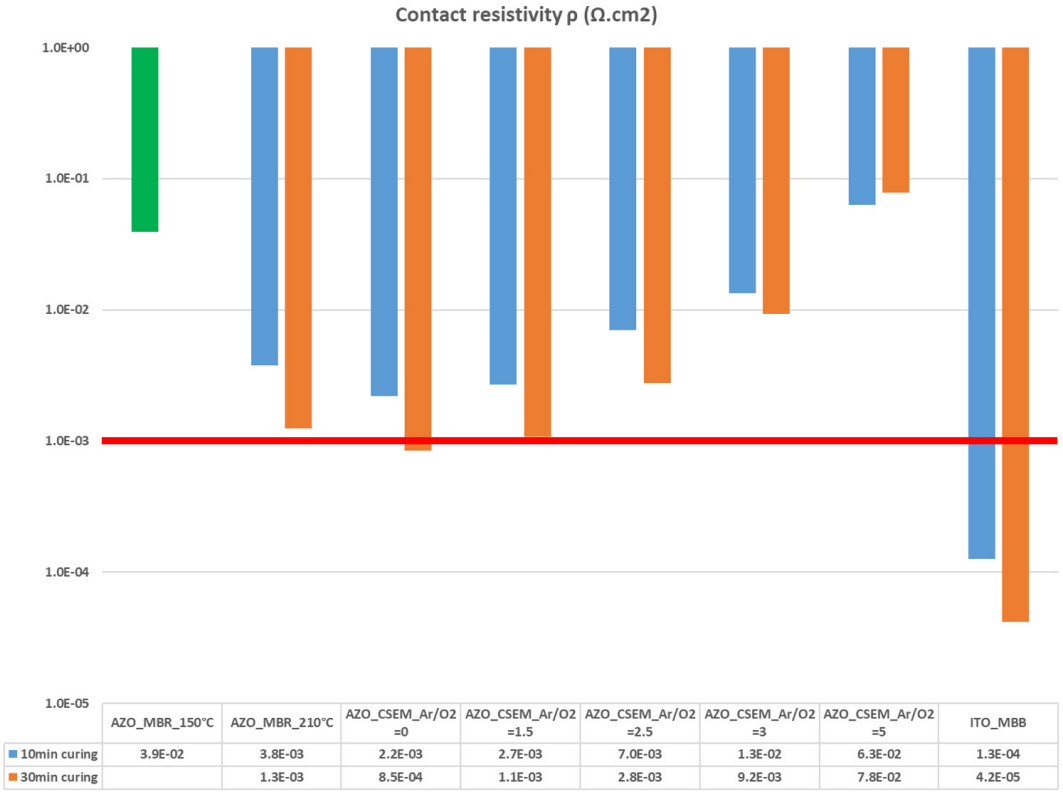


| | AZO_MBR_150°C | AZO_MBR_210°C | AZO_CSEM_Ar/O2 =0 | AZO_CSEM_Ar/O2 =1.5 | AZO_CSEM_Ar/O2 =2.5 | AZO_CSEM_Ar/O2 =3 | AZO_CSEM_Ar/O2 =5 | ITO_MBB |
|---|---|---|---|---|---|---|---|---|
| 10min curing | 3.9E-02 | 3.8E-03 | 2.2E-03 | 2.7E-03 | 7.0E-03 | 1.3E-02 | 6.3E-02 | 1.3E-04 |
| 30min curing | | 1.3E-03 | 8.5E-04 | 1.1E-03 | 2.8E-03 | 9.2E-03 | 7.8E-02 | 4.2E-05 |

Figure 32: AZO splits in comparison with ITO for contact resistivity in 10min and 30min curing conditions.

c) Colorless resin test

To improve the bifaciality of the resin paste, another alternative colorless resin has been tested for the printability and measured for the absorbance in Figure 33.

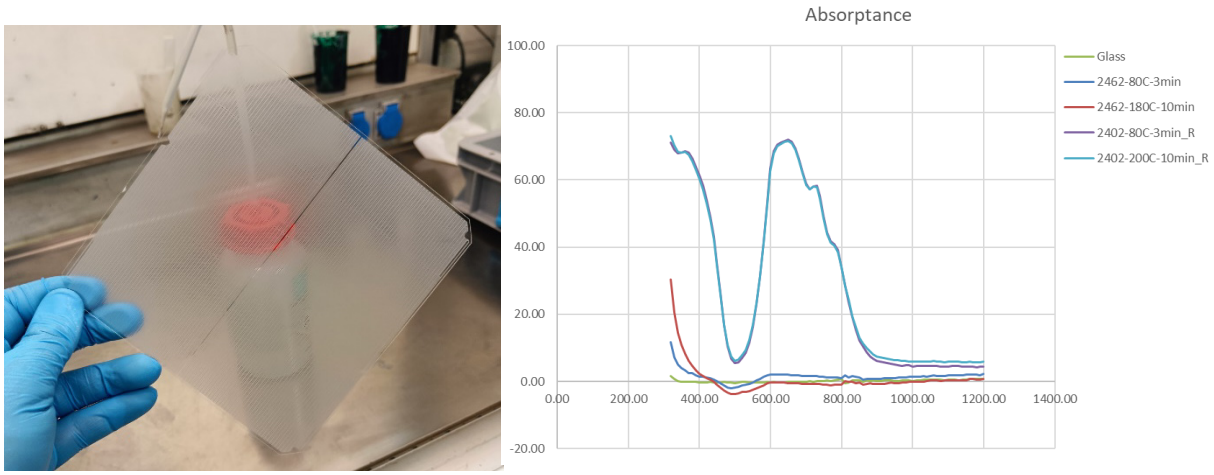


Figure 33: print sample of colorless resin on glass and the absorbance curves

This paste was able to be printed at a speed of 200 mm/s with relatively good printability and this paste seems non-absorbing in almost the entire range of interest wavelengths between 400~1200 nm, therefore is a very good candidate for Bifi application.

d) 2nd 3D finite-element simulation

CSEM went further with the numerical simulations of bifacial IBC devices. As a reminder, the simulated domain is depicted in Figure 34 below. It comprises a half-period in both the horizontal and vertical direction. Importantly for the results discussed below, the number of fingers on the n- and the p-collecting regions can be varied independently. Here, four different bifacial configurations were simulated, with an increasing number of n- and p-fingers, as illustrated in Figure 35. A monofacial version of the IBC (not drawn) was also simulated as a benchmark for the bifacial IBC devices performance.

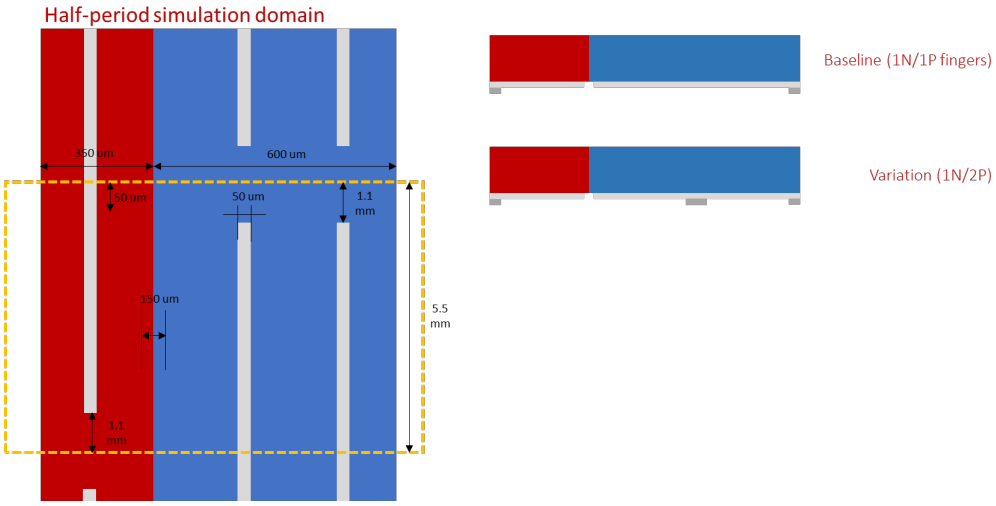


Figure 34: The simulation domain used for the numerical modelling of bifacial IBC devices. Left: rear side view; right: cross-sectional view.

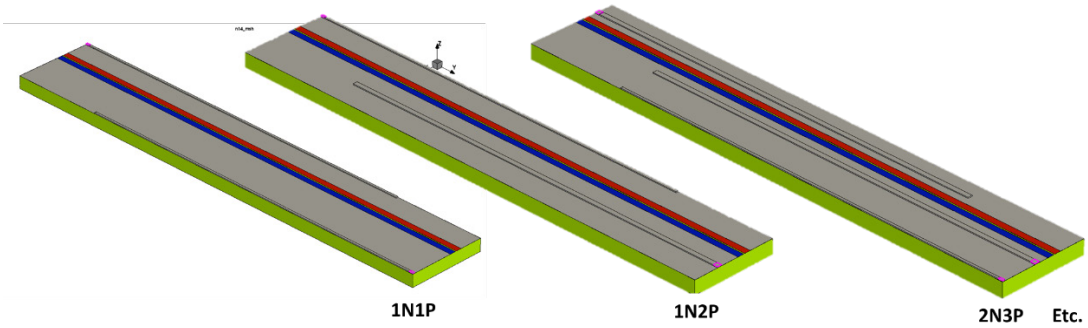


Figure 35 Different rear side designs of bifacial IBC devices, with increasing amounts of fingers on the n- and p-collecting regions (rear side views).

For each rear side design, the performances of the IBC devices under front side or rear side illumination were computed for three different TCO sheet resistances, namely 30, 150, and 300 Ohm/sq, as well as two bulk lifetimes, namely 3 and 30 ms. Note that for the time being, the optical constants of the TCOs are kept the same regardless of the doping, and therefore optical parasitic absorption effects are not captured by the simulations. This owes to the lack of experimental data and the difficulty in precisely measuring the optical constants of TCO materials. In addition, the surfaces are considered as perfectly passivated so far, so no surface recombination effects are implemented in the simulations so far. This will be corrected in the next iterations. Figure 36 shows the variation of the short-circuit current density ($J_{sc}$) as a function of the number of fingers on the rear side of the IBC in case of front or rear side illumination. Expectedly, in case of front side illumination, the $J_{sc}$ of the bifacial IBC device depends only weakly on the number of fingers on the rear side, as those only contribute marginally with light recycling. For these reasons, the fully metallized (hence monofacial) reference IBC device exhibits the highest $J_{sc}$. Turning now to the case of rear side illumination, the $J_{sc}$ is found to rapidly drop when the number of n- and p-fingers increases owing to the direct shadowing provided by these latter. Note that these results are valid for all TCO doping's, as parasitic absorption in the rear TCO is not taken into account yet, as explained above.

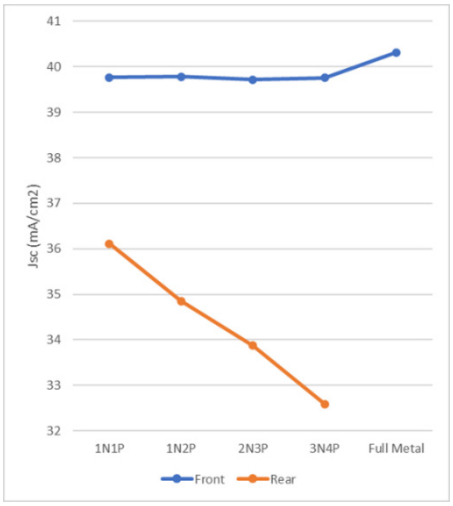


Figure 36 Variation of the short-circuit current density as a function of the number of fingers on the rear side of the IBC in case of front (blue line) or rear (orange line) side illumination.

Figure 37 plots the variation of the fill factor (FF, left part of the graph) and the efficiency (right part of the graph) for the different rear side designs and TCO sheet resistances, in the case of a bulk lifetime of 30 ms. The obtained results are consistent: regardless of the illuminated side, the FF is found to increase with the number of fingers on the rear side and the TCO conductivity.

When looking at the efficiency of the IBC devices in case of front side illumination, their efficiency is found to increase with the number of fingers at the rear side. Said differently, the efficiency in case of front side illumination is mainly driven by the FF, and to a lesser extent by the $J_{sc}$ (see Figure 36 above). Noteworthy, the 1N1P configuration – the most "aggressive" bifacial design – features an efficiency drop of 1% absolute compared to the fully metallized IBC reference. In contrast, the efficiency in case of rear side illumination is found to steadily and rapidly decrease with the number of fingers. This is a direct consequence of the sharp $J_{sc}$ loss seen in Figure 36, which is not compensated by the FF increase.

Note that the trends are essentially similar in the case of a 3 ms bulk lifetime, with all parameters being shifted to lower values owing to the reduced bulk lifetime (data not shown).

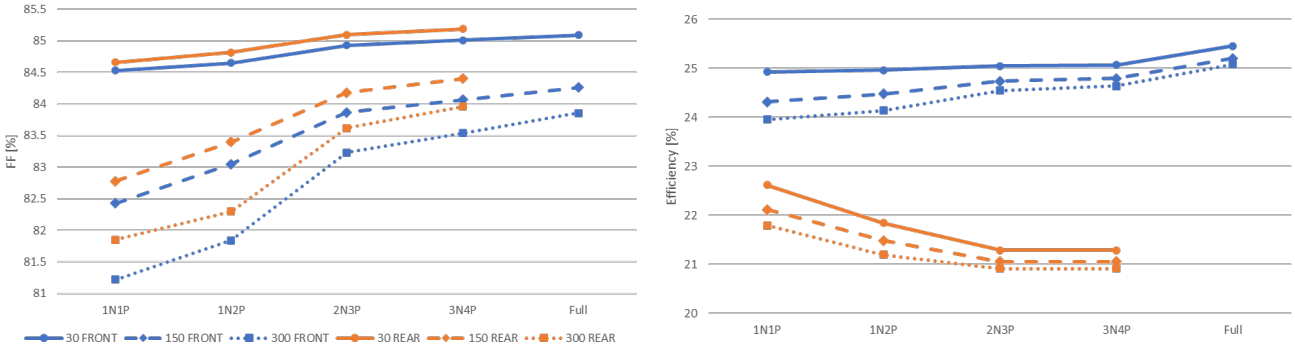


Figure 37: Variation of the fill factor (FF, left part of the graph) and the efficiency (right part of the graph) for the different rear side designs and TCO sheet resistances, in the case of a bulk lifetime of 30 ms.

Finally, we simulated the performance of a bifacial IBC device (assuming the 1N1P rear design) when front and rear illuminations are present simultaneously. This represents what an actual bifacial IBC device would undergo when installed outside. Here, we simulated bifacial boost (β) of 5, 10 and 20 % of the rear $J_{sc}$, which correspond to the typical bifacial effect obtained with PV systems installed on grass or concrete. Here, the total $J_{sc}$ of the bifacial IBC devices reads:

$J_{sc},tot = J_{sc},front + \beta.J_{sc},rear$, where $\beta = 0.05, 0.10, 0.20$

Table 2 below summarizes the results. As can be seen, already with a bifacial boost of 5% of the rear side illumination, the total efficiency of the bifacial IBC device reaches 25.5%, hence the same efficiency as the reference fully metallized IBC device. With even higher bifacial boosts, efficiencies > 28% are within reach.

| | Front | Rear | +5% bifi | +10% bifi | +20% bifi |
|---|---|---|---|---|---|
| Jsc [mA/cm2] | 39.66 | 34.90 | 41.41 | 43.15 | 46.64 |
| Voc [mV] | 741.7 | 739.4 | 742.5 | 743.3 | 744.8 |
| FF [%] | 82.97 | 83.38 | 82.84 | 82.72 | 82.46 |
| Eff [%]/1-sun | 24.40 | 21.52 | 25.47 | 26.53 | 28.64 |

Table 2: Performance of a 1N1P bifacial IBC device for three different bifacial boosts.

e) new AZO+ITO stack layer

In the contact resistivity measurement on 3 samples, a thin ITO as capping layer on the AZO has improved the contact resistance and reached our target of 1 mΩ.cm$^2$ with our baseline curing condition. From this test, we defined our new baseline with AZO and thin ITO capping layer stack as the TCO.

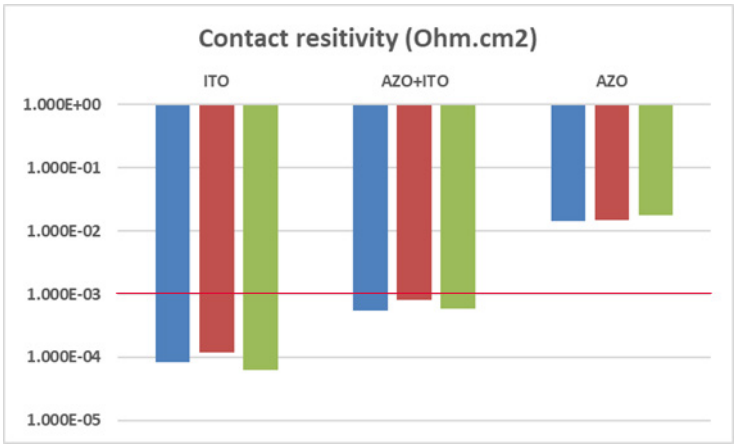


Figure 38: contact resistivity measurement for ITO, AZO+thin ITO stack and AZO

f) finger patterning evaluation

In the comparison test between 2 different finger patterning with 2P1N and 4P2N for standard (1st Resin-2nd Finger) and Fongi concept (1st Finger- 2nd Resin) on cell level. The new AZO+thin ITO stack has been involved in all groups. The experiment plan and part of the pattering are shown below. A group with 'mushroom' as reference was done.

| Group | Finger Layout | Additional Pads |
|---|---|---|
| Mushroom-Ref | - | Thin pads |
| Standard-M like (1st Resin, 2nd Ag) | 2P1N | No |
| Standard-M like (1st Resin, 2nd Ag) | 4P2N | No |
| Fongi (1st Ag, 2nd Resin) | 2P1N | Thin pads |
| Fongi (1st Ag, 2nd Resin) | 4P2N | Thick/large pads |

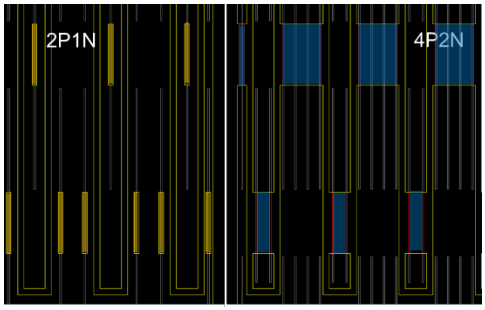


Figure 39: Experiment DoE (left) and the finger patterning 2P1N vs 4P2N

On the LIV parameters, only cell efficiency (ETA in %) and FF as main considered cell parameters have been presented in the Figure 40.

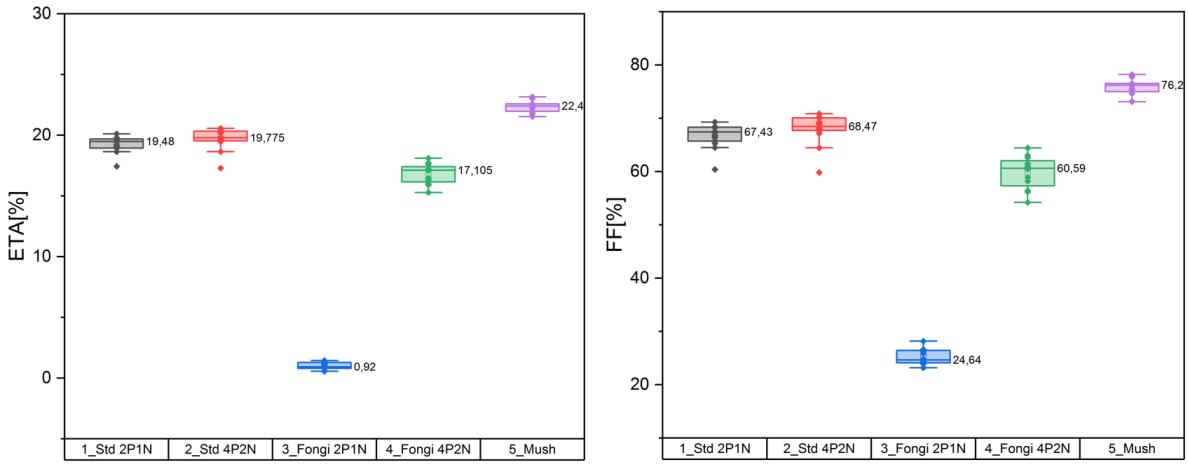


Figure 40: Efficiency and FF boxplots in experiments

The reference group with mushroom has reached relatively usual range for cell efficiency of 22.4 % with acceptable FF in 78.2 % in median. Both groups with standard concept have shown much lower FF with 67-68 % and 3 % lower efficiency. Due to extremely low FF for the group Fongi 2P1N, the cell efficiency was measured very poor. But the Fongi 4P2N group has 2 % lower efficiency than the standard concept. In the further troubleshooting for the extreme low FF for Fongi 2P1N group we observed that the EL was very weak and it means that there wasn't really physical contact between the finger and the thin silver pads. Under the microscope we detected that the large organic spreading of the resin paste covered the silver finger, and the pads above couldn't build contact with the fingers, which explained the root cause of the poor FF and efficiency of this group.

On the module level, we observed astonishing improvement of 6-8 % absolute FF for the Fongi 4P2N group from cell to module and the results are demonstrating in the table and Figure 41 below. The final module efficiency of the Fongi 4P2N finger patterning was even close to the mushroom baseline.

| | ref | Eff[%] | Voc[mV] | FF[%] | Jsc[mA/cm2] |
|---|---|---|---|---|---|
| cell | WO9466_35T | 18.11 | 739.2 | 64.42 | 38.03 |
| Module | 506193 | 19.16 | 734.6 | 70.84 | 36.81 |
| CTM(%) | | 5.8 | -0.6 | 10.0 | -3.2 |

| | ref | Eff[%] | Voc[mV] | FF[%] | Jsc[mA/cm2] |
|---|---|---|---|---|---|
| cell | WO9466_42T | 17.22 | 739.2 | 61.47 | 37.9 |
| Module | 506194 | 19.04 | 735.8 | 69.58 | 37.18 |
| CTM(%) | | 10.6 | -0.5 | 13.2 | -1.9 |

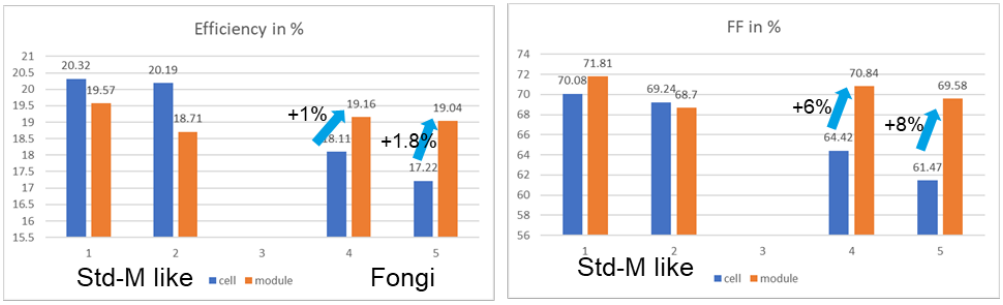


Figure 41: Fongi cell and module parameters, strong improvements in FF from cell to module

It means that the IV test has underestimated the cell parameters due to insufficient contact between the chuck and the metal fingers physically. A relatively high bifaciality of almost 70 % high level was measured on the Fongi group in current density and the results are presented in Table 3.

| | module name | Jsc[mA/cm2] front | Jsc[mA/cm2] back | Bifaciality[% |
|---|---|---|---|---|
| Std Bifacial | 506191 | 37.14 | 21.47 | 57.82 |
| Std Bifacial | 506192 | 37.08 | 21.14 | 57.01 |
| Fungi | 506193 | 36.81 | 25.54 | 69.39 |
| Fungi | 506194 | 37.18 | 25.81 | 69.40 |

Table 3. Bifaciality measurements on the mini-modules, almost 70% bifaciality achieved on Fongi cells

g) improvement to minimize organic spreading of transparent resin paste

In the previous tests 1st version of resin paste caused relatively high organic spreading and it impacted not only the contact between silver finger and pads and the etching process strongly. We knew from our process optimization experience on classic heterojunction solar cells that the small pyramid size from texturing can lead narrower finger width during the screen printing step. To minimize such organic spreading of resin, by involving different additive for texturing process we introduced a test split with standard and smaller pyramid sizes and tested the samples with an improved version of transparent resin for less spreading.

The Figure 42 below demonstrates the difference of 2 different pyramids sizes. The smaller pyramids achieved in mean value of 300 nm and larger pyramids in range of 900 nm.

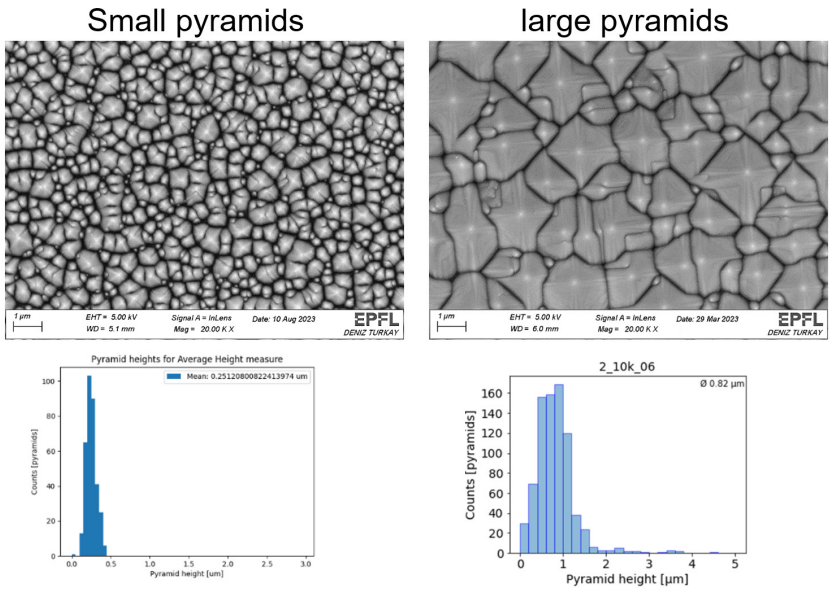


Figure 42: comparison of 2 different pyramids sizes and the distribution of pyramids, large pyramids were applied as the baseline condition.

After the screen printing for the 2nd version of transparent resin and silver paste with 300 mm/s high print speed we observed a gap between 2 resin areas on smaller pyramids sample were relatively larger under 200 mm/s print speed, but not significantly difference under 300 mm/s print speed in Figure 43.

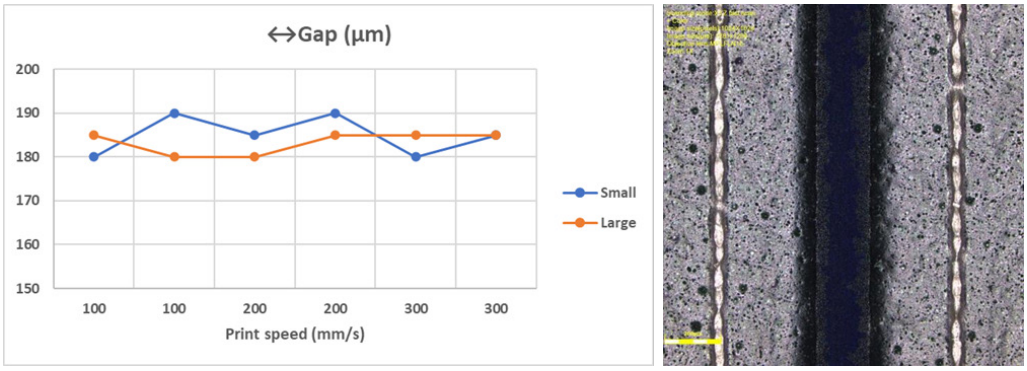


Figure 43: gap after printing the 2nd version of resin paste in 2 print speed under 200 µm opening

To compare with the 1st version of transparent resin, under the microscope we observed that the opened area under 100 and 300 mm/s speeds is much larger than the same condition with 1st version resin in Table 4.

| Transparent Resin | Substrat | Print speed (mm/s) | N->P Open gap (200 µm) |
|---|---|---|---|
| 1st Version | AZO + ITO | 100 | 105 |
| | AZO + ITO | 300 | 115 |
| 2nd Version | AZO + ITO | 100 | 180 |
| | AZO + ITO | 300 | 185 |

Table 4. Comparison of the gap distance in µm between 2 versions of resin pastes

However, Figure 44 shows the smaller pyramids lead a significant reduction in silver paste laydown of around 30 mg. It could save the silver consumption potentially in mass production.

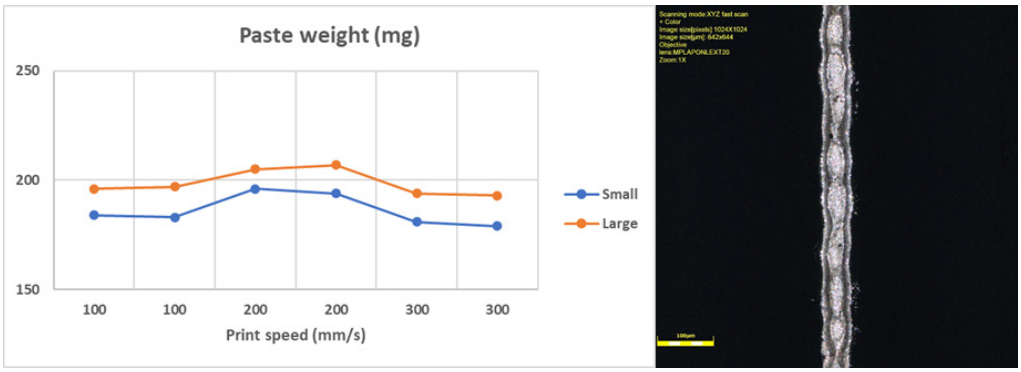


Figure 44: metal consumption in 2 pyramid sizes from 100 to 300 mm/s print speed (left) and metal finger geometry under microscope.

In the etching test, this new transparent resin for less spreading resulted also much less etching time than the 1st version.

h) further optimization on finger patterning

From our last simulation and also last experiment on cell level we learned that more fingers could improve the FF due to better lateral transport between the ITO and metal fingers. To achieve higher FF we have increased the finger amount from 4P2N to 5P3N in the new finger pattering in Figure 45.

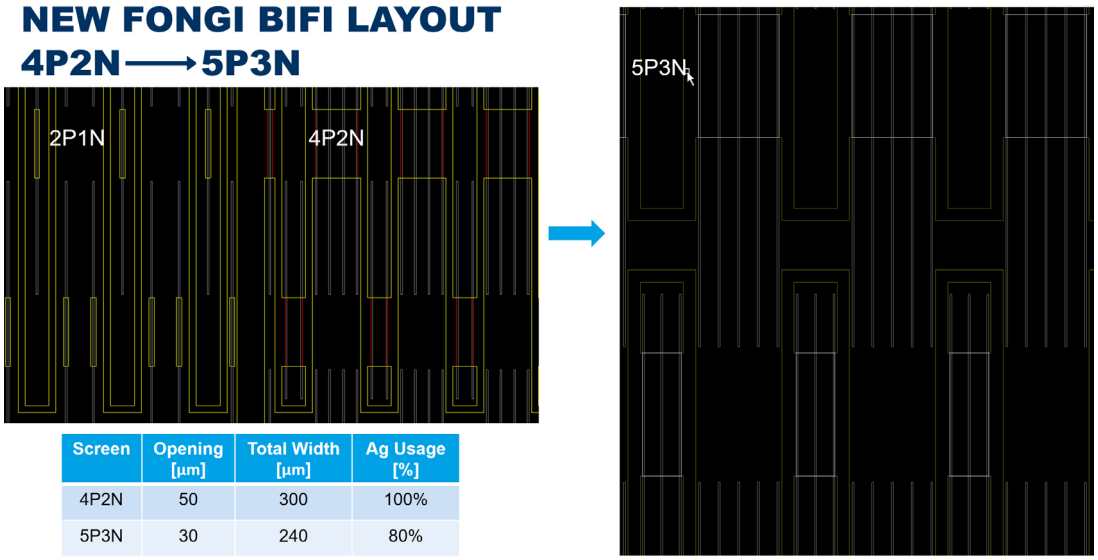


| Screen | Opening [µm] | Total Width [µm] | Ag Usage [%] |
|---|---|---|---|
| 4P2N | 50 | 300 | 100% |
| 5P3N | 30 | 240 | 80% |

Figure 45: new design of Fongi finger pattering with 5P3N for higher FF and 20 % silver saving

Usually with increased finger amount, the silver consumption will be increased proportionally. But in our new finger pattering, we introduced narrower finger opening with 30 µm instead of 50 µm, which means that we could even save 20% silver consumption with more fingers for higher FF.

## 2.2 Module pilot line (WP3)

### 2.2.1 Bill-of-materials (BOM) development for glass-glass modules (CSEM, M1-M24) (Task 3.1)

During of the full project, CSEM developed and tested many different BoM for the implementation of MBR IBC HJT cells into highly reliable modules. The different tests included varying interconnection dimensions (wires diameters, wires coatings), foils materials and designs, encapsulants (TPO, POE) with various WVTR and OTR values, module back layer (backsheet with and without Aluminium, or glass), as well as varying cells backend materials, processes and designs (including the objectives to minimize Silver usage while keeping highest performance and reliability). For all these BoM, we performed various extended reliability testing, including thermo-cycling, damp heat or humidity freeze, to determine the best combination that can achieve high reliability performance.

To achieve this goal, CSEM built more than 1500 mini-modules all along the project based on either M2, HM2 or 2xHM6 wafers size, the latter being the most used platform to develop the module BoM. As of today, the status is that the current BoMs developed can easily pass 3 times the IEC norm concerning thermo-cycling, damp heat and humidity freeze (Figure 46, 47 and 48). It means:

- 600 cycles of thermos-cycling between -40°C and 85°C.
- 3000 hours of damp heat at 85°C and 85% humidity rate
- 30 cycles of humidity freeze between -40°C and 85°C (with 85% humidity rate at 85°C)

The current BoM (BoM V2) is composed by:

- 1 front glass
- 1 x layer of UV through encapsulants based on POE polymer (Polyolefin elastomers are a range of copolymers based on metallocene catalysis utilizing butene or octene comonomers).
- HJT IBC tunnel junction cells (several half M6 cells) with Ag printed metallization at the back and polymer-based resin (as an insulator between polarities)
- SmartWire interconnection: composed of 300 µm diameter wires and a low melting point alloy based on Bismuth.
- A multi-layer foil based on PO polymer (polyolefin) to follow the specifications of the FWA (foil wires assembly) functionalities. This development of a new foil was performed in a previous CTI project named DEFIA.
- Thicker encapsulant of same polymer type used in front side but with UV blockers particles to protect the backsheet.
- An aluminium backsheet to limit the water ingress in module and reducing the final weight of the module.

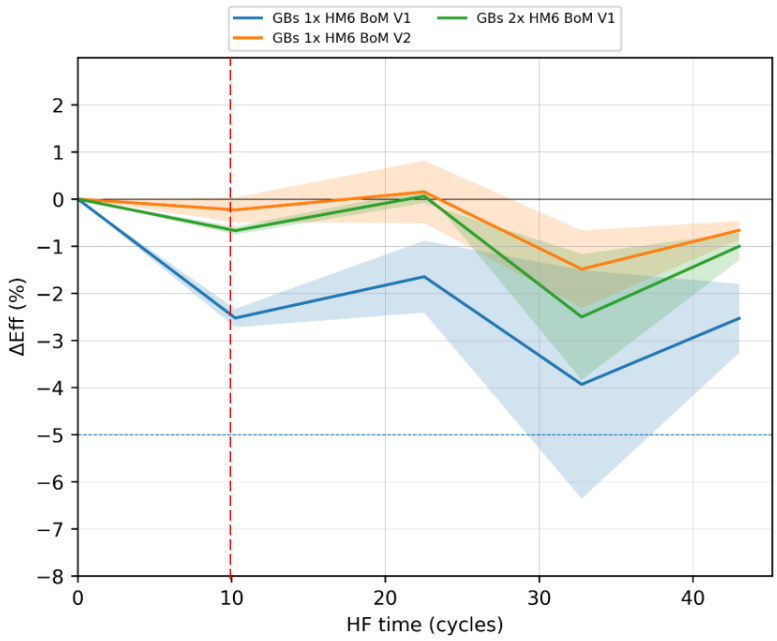


Figure 46: Humidity Freeze (HF) degradation after more than 4x IEC norm for the new standard BoM (V2) and the previous (V1).

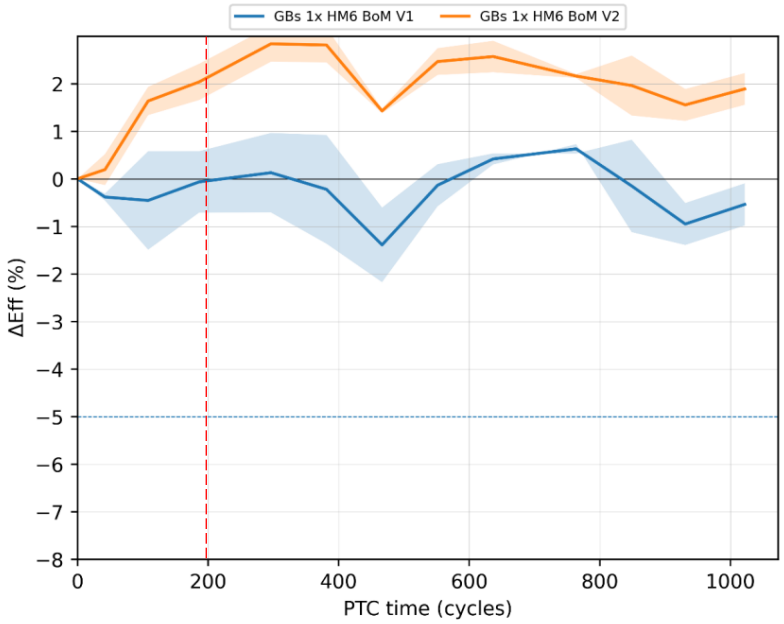


Figure 47: Thermo-cycling (PTC) degradation after more than 5x IEC norm for the new standard BoM (V2) and the previous (V1)

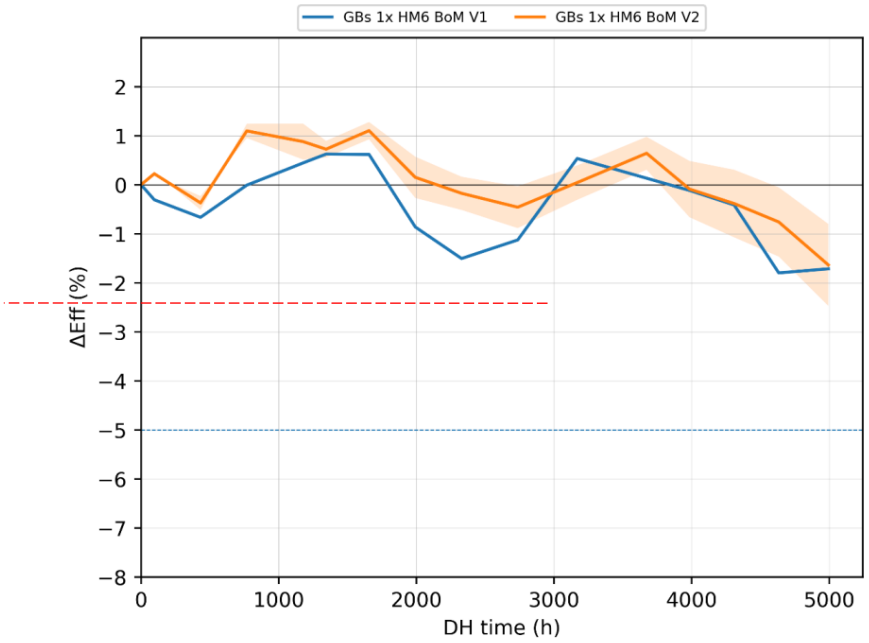


Figure 48: Damp Heat (DH) degradation after 5x IEC norm for the new standard BoM (V2) and the previous (V1)

These demonstration results are key achievements for a future industrial product with a unique reliability potential. Therefore, the SIRIUS objectives to achieve a minimum of 30 years reliability are fully achieved.

Meyer Burger with CSEM and other partners are involved in the European project PILATUS, where the degradations mechanism for the developed BOM are being pushed further for a deeper understanding of the physical mechanism (i.e. when/how it appears). Further tests not covered within SIRIUS are being addressed such as the reliability against UV degradation, potential induced degradation (PID) degradation as well as consecutives and extended stress tests.

With the high reliability of new standard BoM (V2) being achieved, CSEM and MBR decided to push in the final year of the project to further decrease the cost of this BoM while conserving the high reliability. The current market situation shows that changing the backsheet is a first way to decrease the cost. In that respect, backsheet without aluminium inside and glasses are less expensive than the backsheet with Aluminium sheet inside used in the defined BoM. First efforts were therefore dedicated to the evaluation and development of a BoM without Aluminium in the backsheet. The results demonstrate that water vapor and oxygen ingress are not causing too strong and fast degradation of the developed IBC cells, as clearly demonstrated with the degradation results observed in the case of no backsheet. It is believed that the cell backend combined with the SmartWire foil and back encapsulant provide already an efficient encapsulation of the solar cells. This enables to have modules demonstrated to pass 3 times IEC norms without any backsheet, or with a backsheet without Aluminium. It must be noted that this results is outstanding for HJT contact based devices, and not achieved in the case of traditional HJT solar cells, therefore clearly demonstrating that IBC HJT devices developed are more stable and resilient to external environmental stresses than traditional HJT devices.

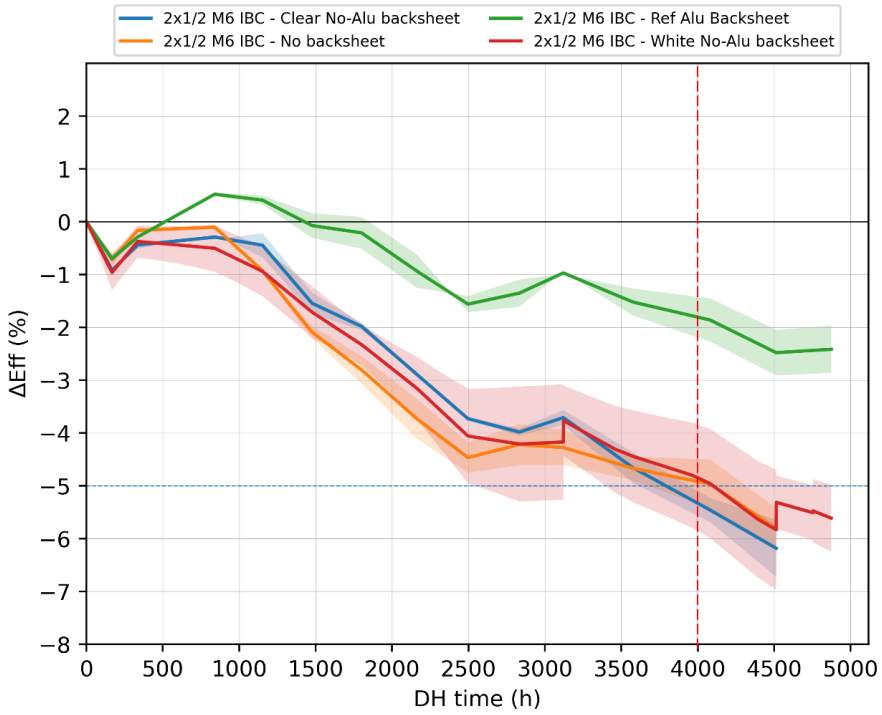


Figure 49: Damp Heat (DH) degradation after more than 3x IEC norm for the modules without Aluminium backsheets compared to standard BoM (V2) containing aluminium backsheet.

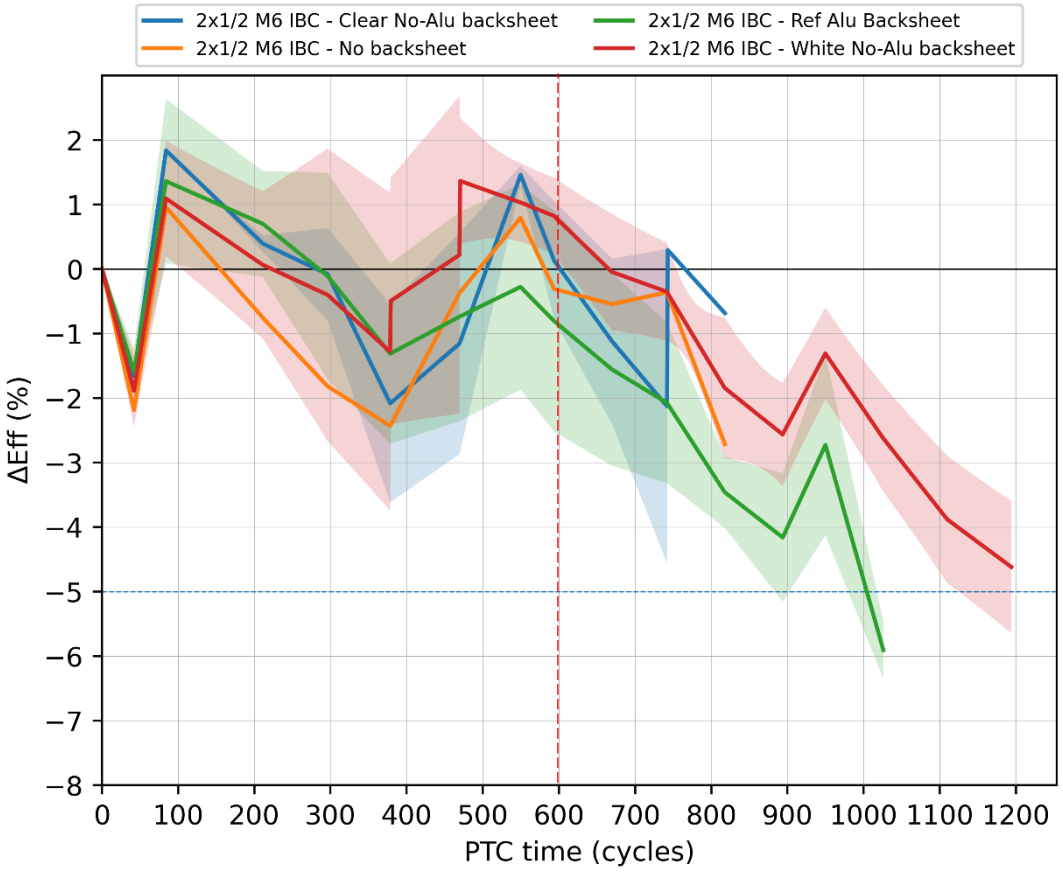


Figure 50: Thermo-cycling (PTC) degradation after more than 5x IEC norm for the modules without Aluminium backsheets compared to standard BoM (V2) contained aluminium backsheet.

As highlighted in Figure 49 and 50, combining non-Aluminium backsheets leads to reach 3x the norm requirements for DH and TC. In DH, the degradation is higher for the no-aluminium backsheet compared to the Aluminium reference backsheet. Even no backsheet is passing DH conditions. No differences are observed in PTC conditions.

CSEM implemented other new modules materials to decrease the manufacturing cost of the module, also involving new cell back-end cell materials at lower cost developed by MBR. CSEM integrated MBR cells with various low Ag content metallization pastes in module. The concentration of Ag in the metallization paste can vary from 60% to below 30% compared to the reference at 90% of Ag content.

| Metallization pastes | % of Ag content |
|---|---|
| Ref | 90 |
| M12 | 53 |
| M7 | 47 |
| M13 | 46 |
| M6 | 45 |
| M14 | 40 |
| M8 | 37 |
| M10 | 30 |
| M9 | 28 |

Figure 51: Metallization paste list with the percentage of silver (Ag) content.

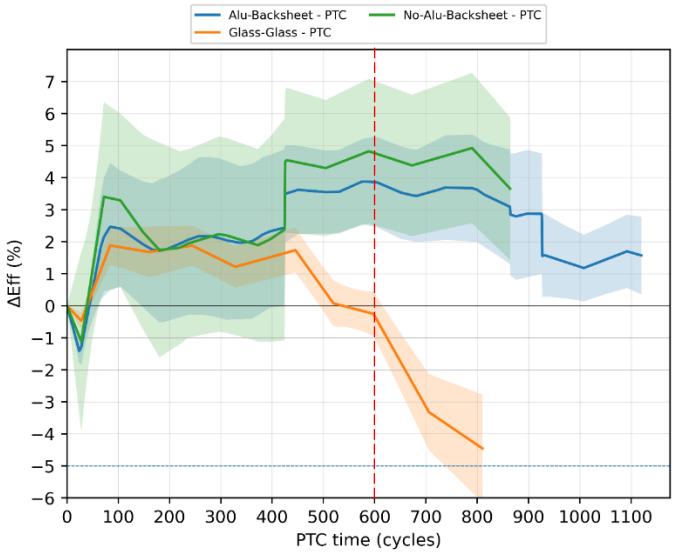


Figure 52: Thermo-cycling (PTC) degradation after more than 3x IEC norm for the modules integrating low Ag pastes in various BoM configurations.

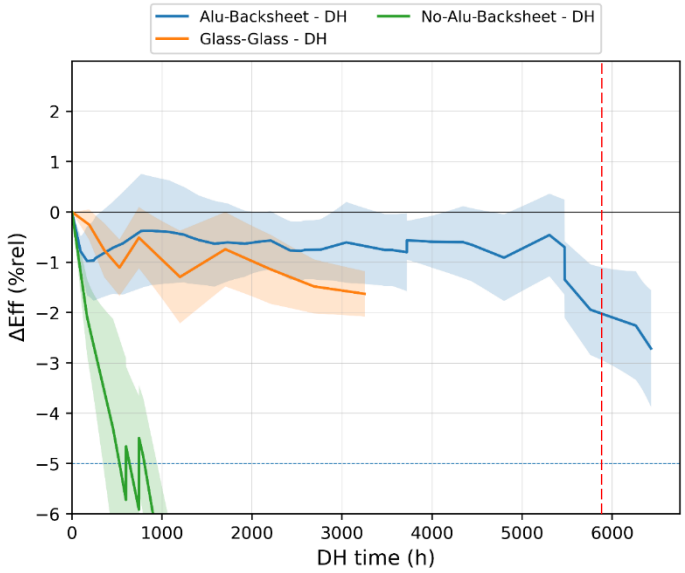


Figure 53: Damp Heat (DH) degradation after more than 3x IEC norm for the modules integrating low Ag pastes in various BoM configurations.

Combinations of material reduction were further tested, e.g. combining low Ag metallization pastes together with non Aluminium backsheet. However, low Ag metallization pastes are more sensitive to water ingress, resulting in important losses when implemented in modules with Backsheet without Aluminium. Using a backsheet with aluminium or glass with low Water Vapor Transmission Rate (WVTR) reduce consequently the losses in DH and is therefore shown to be necessary if implementing such low Ag pastes. As visible on Figure 54 in thermos-cycling, some losses were observed on glass-glass modules after 50 cycles due to different batches of cells with a process issue presented later.

Now, MBR integrated them in the last version of the IBC cells especially for the glass-glass module and the glass-Alu-Backsheet module BoM selected. Regarding the back side of the module, the current market situation shows that glass is more competitive to backsheet (even without alu). In agreement with Meyer Burger, we integrated glass as backsheet of the module. CSEM helped Meyer Burger Research to determine keys processing parameters to be controlled for the industrialisation of the HJT IBC technology. CSEM was able to help Meyer Burger to define curing time for the back end insulator resin after MBR changed their curing furnace, demonstrating the impact of curing time onto reliability.

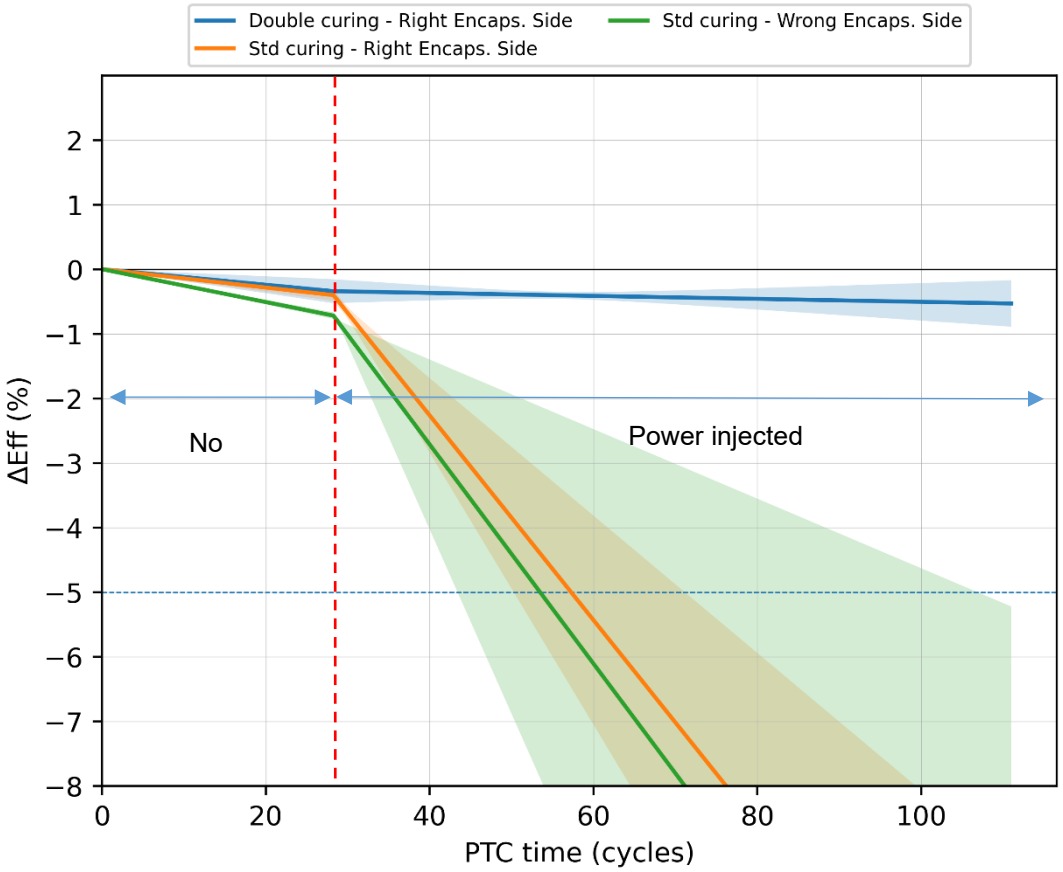


Figure 54 Thermo-cycling (PTC) degradation showing impact of the cell curing process on module reliability.

The last part of SIRIUS development from CSEM, was dedicated to decrease the critical raw materials (CRM) used in wires (Bi, In, PB…). CSEM integrated new wires with lower cost coating, Bismuth free, Indium free, Silver free and Lead free and test them in reliability.

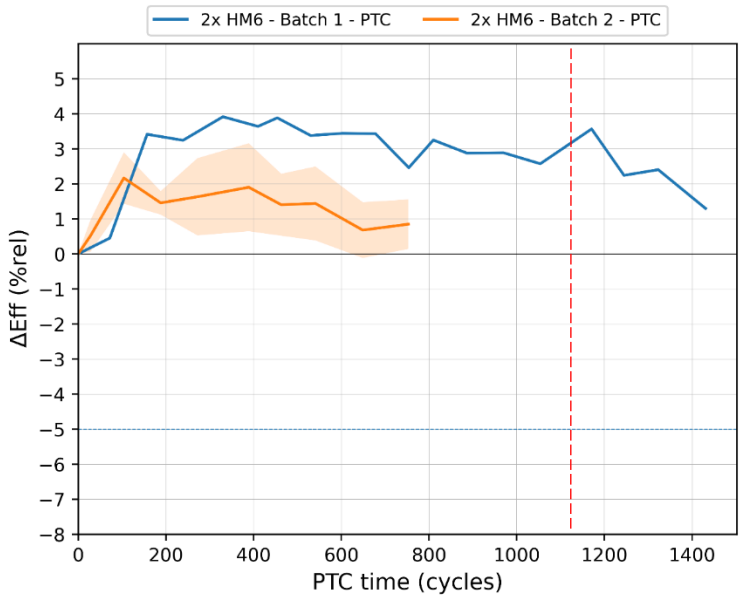


Figure 55: Thermo-cycling (PTC) degradation after more than 3x IEC norm for the new standard BoM (V2) combined with wires containing no CRM in the coating.

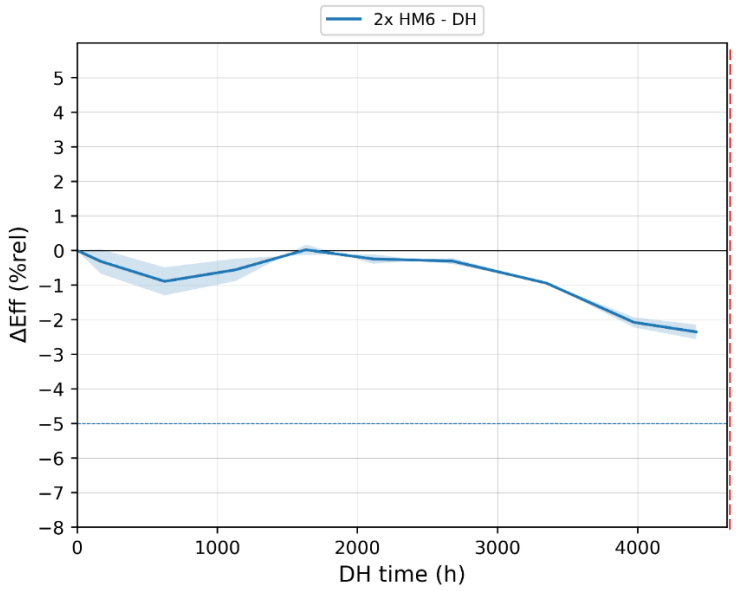


Figure 56: Damp Heat (DH) degradation more than 3x IEC norm for IBC modules with the new standard BoM (V2) combined with wires containing no CRM in the coating.

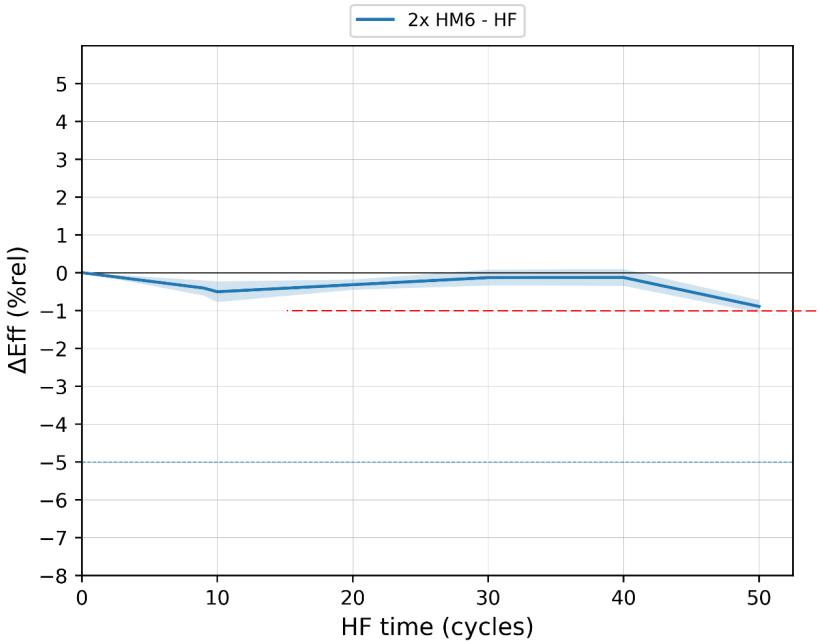


Figure 57: Humidity Freeze (HF) degradation after more than 4x IEC norm for with the new standard BoM (V2) combined with wires containing no CRM in the coating.

For all the reliability tests performed, no degradation of performance was observed for more than 3x IEC norms requirements. These results demonstrate for the first time highly reliable PV modules based on silicon wafer solar cells, without soldering or conductive adhesive, but solely mechanical contacting. These results are outstanding, and demonstrate the high reliability that can be achieved with the technology at the end of the SIRIUS project.

The module implementation of MBR IBC HJT cells done at CSEM during the SIRIUS project lead to highly impressive results, surpassing the initial objectives of the project and demonstrating the high potential of the IBC HJT – SmartWire technology, surpassing performance and reliability of HJT SmartWire technology. Several bill of materials were defined and demonstrated, and paths for costs reductions clearly demonstrated.

In addition, applications of IBC HJT cells for special PV modules were evaluated.

First, CSEM demonstrated the possibility to integrate the HJT-IBC solar cells in glass-free lightweight modules. The modules demonstrated weight < 2 kg/m$^2$, and excellent performance and reliability. The compatibility was therefore demonstrated for such alternative product integration.

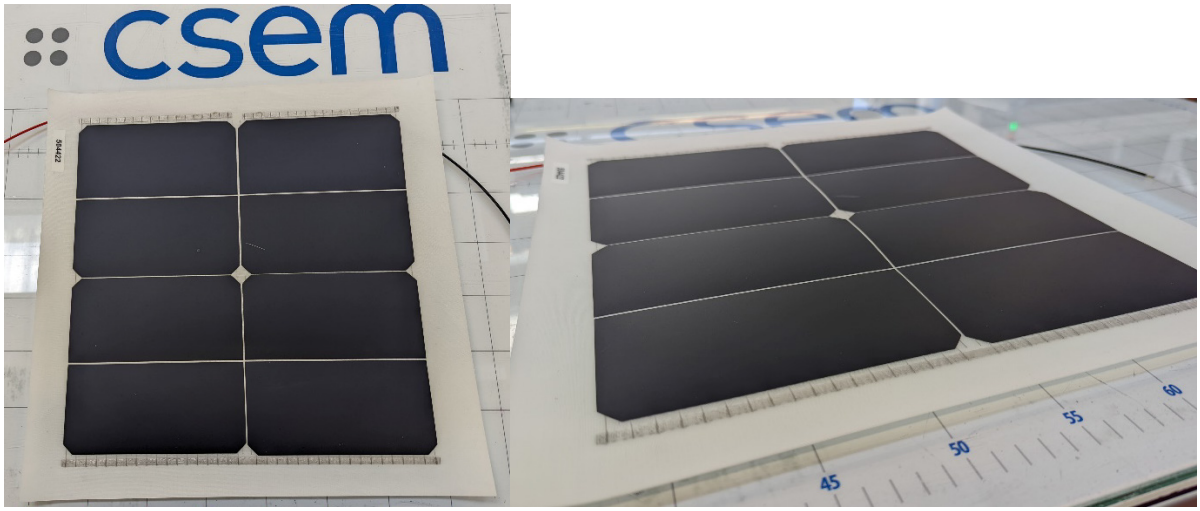


Figure 58: 1st 8x HM6 cells modules built with the lightweight BoM of CSEM.

Secondly, CSEM tested the implementation of colored encapsulant together with IBC HJT cells. Here again, excellent compatibility could be demonstrated. The aesthetics are drastically improved with respect to traditional both sides contacted cells with ribbon interconnection as highlighted in Figure 59. Thanks to the uniform color rendering of the IBC HJT solar cells, and to less thickness variations on the front side of the solar cell, higher uniformity can be easily achieved, and no visibility of the solar cells. The developed IBC HJT SmartWire technology is therefore shown to be highly suited for BIPV modules for façade or rooftop integration.

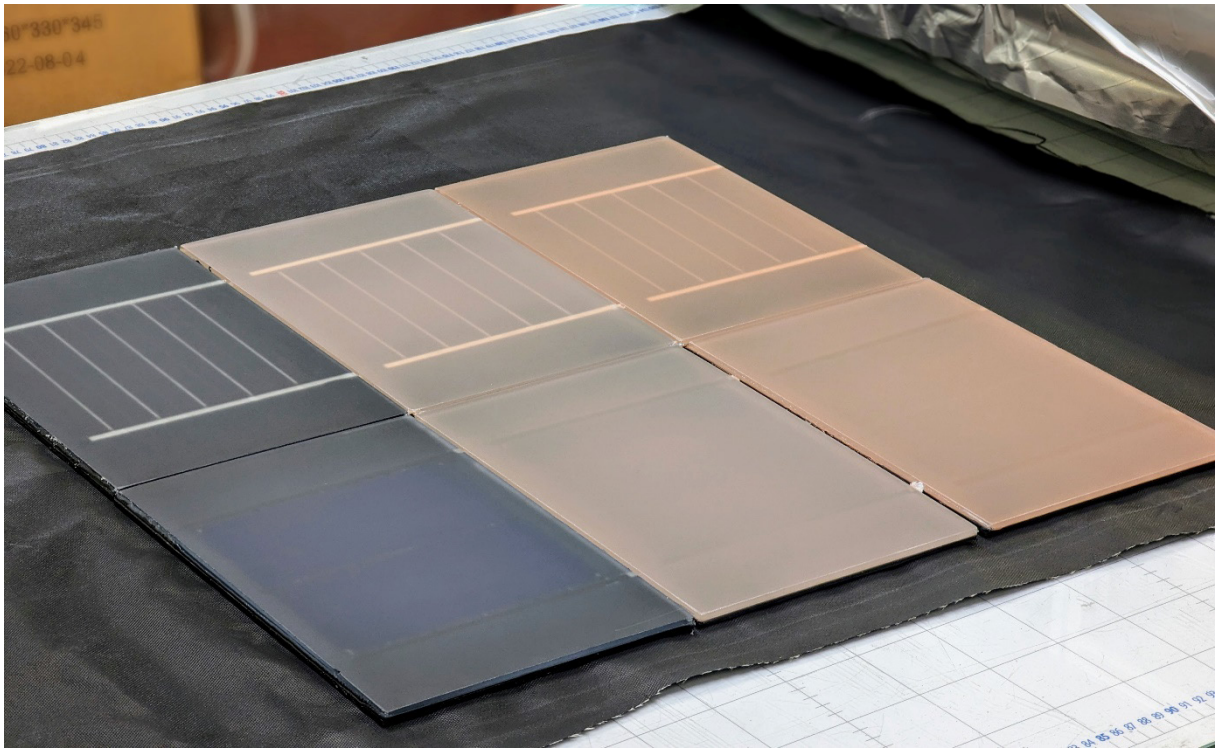

Figure 59: 1st 2x HM6 cells modules built with the Colored BoM and compared to standard cells technology integrated.

### 2.2.2 Development of SWCT® key equipment for tunnel-IBC SWCT® module production (MB-AG, M1-M20) (Task 3.2)

a) Prototype RRU for tunnel-IBC (industrial relevant zero-series) (MB-AG, M1-M18):

In month 18 the deliverable 3.2 was finished with prototype build of the IBC roll-to-roll unit. The factory inspection passed according to machine specification and all FWA (foil-wire-assembly) for module build of deliverable 3.5 (Figure 62: Combined test flow IEC 61215 and IEC 61730; from: Rettest Guideline IEC TS 62915, Ed. 2.0, 2023-09) have been produced on this machine since. For this purpose, the foil cutting unit and transport components were modified to handle a newly developed SWCT foil that promises enhanced reliability and longevity.

b) Prototype CCS for tunnel-IBC (industrial relevant zero-series) (MB-AG: M3-M20):

During the first phase of Sirius, we described how the development platform for the industrial relevant zero-series (CCS FUMU) was converted into a fully functional prototype machine. Since this deliverable (D3.3) in month 20 we have changed the string transport concept from a vacuum belt to a vacuum stepping unit in order to encounter variations in cell-to-cell gaps. The new method was proven successfully by the string production for pre-certification modules. The final prototype design was frozen and construction of the mass production CCS in M10 configuration is ongoing for the successor project PILATUS.

### 2.2.3 Upscaling, production and pre-certification of large tunnel-IBC SWCT® modules (MB-AG, M12-M36) (Task 3.3)

The produced modules reported were tested in climatic chambers at MB-AG and CSEM. Extended test conditions of multiple IEC test cycles were shown already in task 3.1 on mini module level. The recent test results demonstrate that upscaling from mini module to full size module is possible without technical concerns. The bill of material (BOM) was slightly changed: mini modules were built using a newly developed SWCT foil that promises enhanced longevity. In contrary, for the first batch of large scale modules Meyer Burger`s SWCT foil for mass production was used. In the meantime, the machines were modified for handling also the new foil type with the intention of reaching an additional reliability boost.

| |
|---|
| Front glass 3.2 mm with ARC (anti reflecting coating) |
| Front encapsulant, single layer POE without UV blocker |
| Cell matrix of 120 half cells HJT IBC tunnel junction (with Ag print metallization) |
| Cell interconnection via FWA: 300µm Bi-alloy coated wires, industrial relevant polymer SWCT-foil |
| Rear encapsulant, double layer POE with UV blocker |
| Backsheet with integrated aluminium layer as superior water ingress resistance |
| Aluminium frame and 2 part junction box |

Table 5: BOM components of modules for reliability testing

The modules were tested multiple times to IEC requirements as shown in Table 6. Fail criteria are a maximum power degradation of 5% after one time IEC along with fully functionality after climatic chamber tests (insulation and wet-leakage tests). Furthermore, no delamination or severe forming of air bubbles are allowed for visual inspection. All modules passed the test criteria under extended conditions including electrical insulation tests and visual inspection.

| Test | IEC conditions | IEC duration | MB duration |
|---|---|---|---|
| TC<br>Thermal Cycling | Temperature cycle between -40°C and +85°C,<br>powered with Imp during T ramp-up | 200 cycles<br>(1 cycle ~4-5 h) | 960 cycles |
| DH<br>Damp Heat | 85°C,<br>85% relative humidity (r.H.) | 1000 hours<br>(42 days) | 4000 hours |
| HF<br>Humidity Freeze | 85°C; 85% r.H.,<br>1 freezing cycle for 1 hour per day down to -40°C | 10 cycles<br>(10 days) | 50 cycles |
| ML<br>Mechanical Load | minimum test load of 2,4 kPa,<br>positive (downward) and negative (upward) | +/- 2.4 kPa<br>1 hour each | + 5.4/-3.2 kPa<br>1 hour each |

Table 6: Test conditions according IEC and extensions at Meyer Burger

The power increase of the modules after the first thermal cycles (Figure 60) is caused by a current soaking effect. This phenomenon was observed only on TC modules as these modules are powered via an external power supply during the ramp-up phases; see Table 6. A high current induced by light or an external power supply will primarily improve the serial resistance and thus the FF, resulting in a power gain at the beginning but reaching a plateau after a while. This effect was also observed on cell level and is more pronounced on lower cell efficiency classes. For future module characterization a pre-conditioning protocol was defined to stabilize module performance. This allows for high repeatability of IV measurements for direct comparison before and after chamber treatment. Nevertheless, strong module stability can still be observed by the relative change over multiple IEC cycles when comparing the peak values with the final results.

Modules from HJT production lines are monitored frequently for durability. The average reliability performance, resulting from 2 years mass production of Meyer Burger`s facilities in Germany, are displayed as reference (Figure 60) (note: the reference curve for PTC was lifted by 3 %, allowing for direct comparison to module results with current soaking effect). Based on this foundation, Meyer Burger issues a product warranty of 25 years for HJT glass-backsheet products with a guaranteed power performance of 80 % at the end of the life cycle. IBC modules show obvious enhancement compared to the reference lines. Taking further improvement by implementing the newly developed SWCT foil into account, we are positive to foresee a lifetime of 30 years+ for IBC modules.

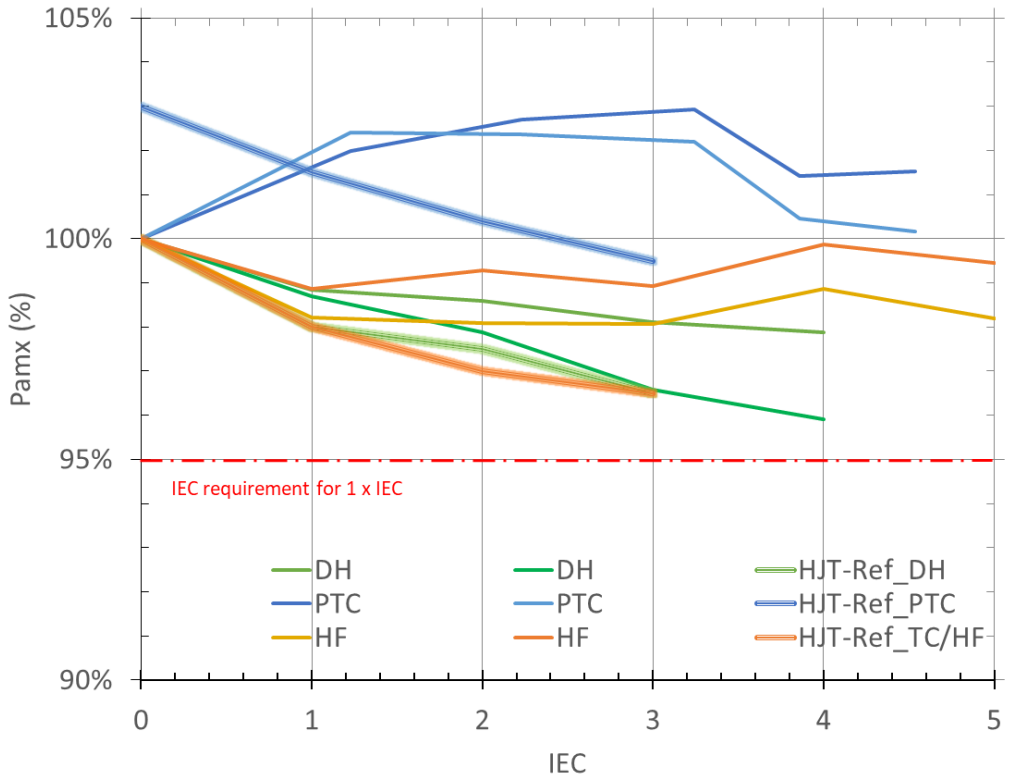


Figure 60: Large size IBC module performance after climatic chamber test of multiple times IEC test conditions

The second batch of twelve large scale modules was produced for outdoor installations at InnoParc. Same BOM as shown in Table 5 was used with the exception of an upgrade to the new developed SWCT foil for extended longevity. For this module production two types of cells were delivered:

(i) IBC cells with Ag-paste metallization comparable to the cells listed in Table 5
(ii) A second cell batch using novel Cu-Ag pastes.

With the latest cell delivery, 21 more modules were built for pre-certification. IBC cell metallization and BOM were the same as for outdoor testing (ii). Available cell efficiencies ranged from 22.8 to 23.8 %. The aim of 400 Wp could not be reached with this cell efficiency but the best module performed at 394 Wp close to the targeted objective. With an average power cell to module loss of less than 1 %, only a slight increase in cell efficiency is required to exceed the 400 Wp mark.

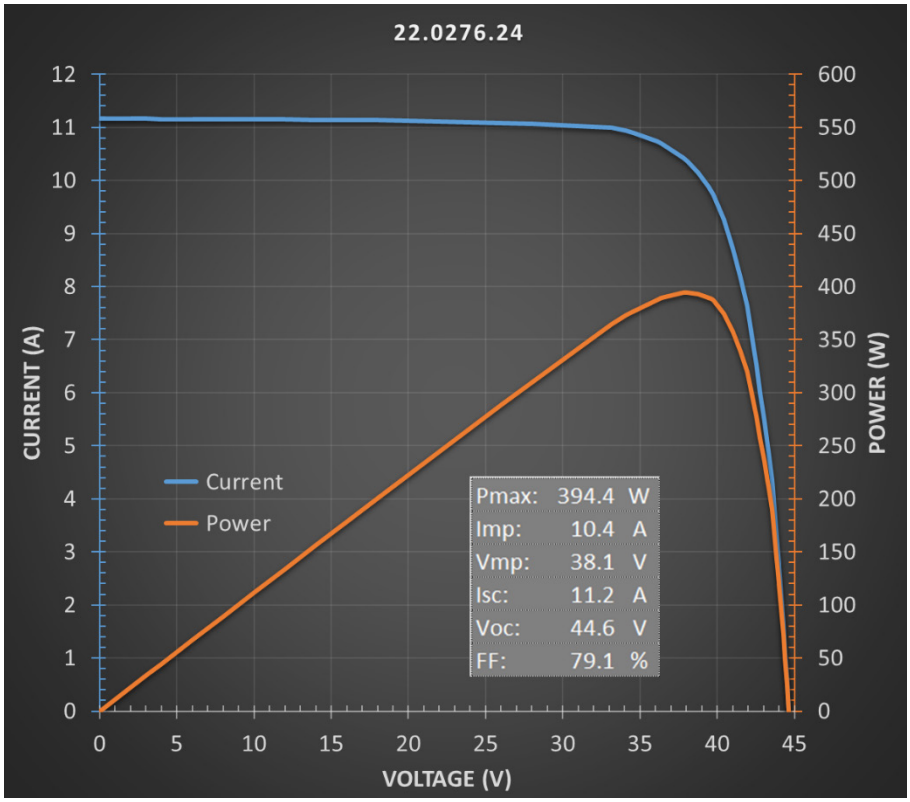


Figure 61: IV and power curve of IBC module with BOM as per Table 5

A full baseline certification of a new product subjected to IEC 61215 / 61730 and UL 61730 enfolds 16 - 18 modules, depending on national regulations. The pre-certification is performed at Meyer Burger`s VDE-accredited Quality & Certification Laboratory (QCL) in Freiberg, Germany. All tests are performed conforming the standard regulations. An extract of the most relevant tests was chosen for the pre-certification displayed in Table 7.

Table 7: selected test for pre-certification according combined tests flow of IEC 61215 and IEC 61730

| pre-certification test IEC 61215 / 61730 | # modules |
|---|---|
| Combined Sequence B/F | 1 |
| Combined Sequence C/C | 2 |
| Combined Sequence D/E | 2 |
| Combined Sequence E/D | 2 |
| IEC61215 Sequence F | 2 |
| IEC61730 Sequence B | 2 |
| IEC61730 Sequence B1 | 1 |
| IEC61730 MST32 | 1 |
| Total: | 13 |

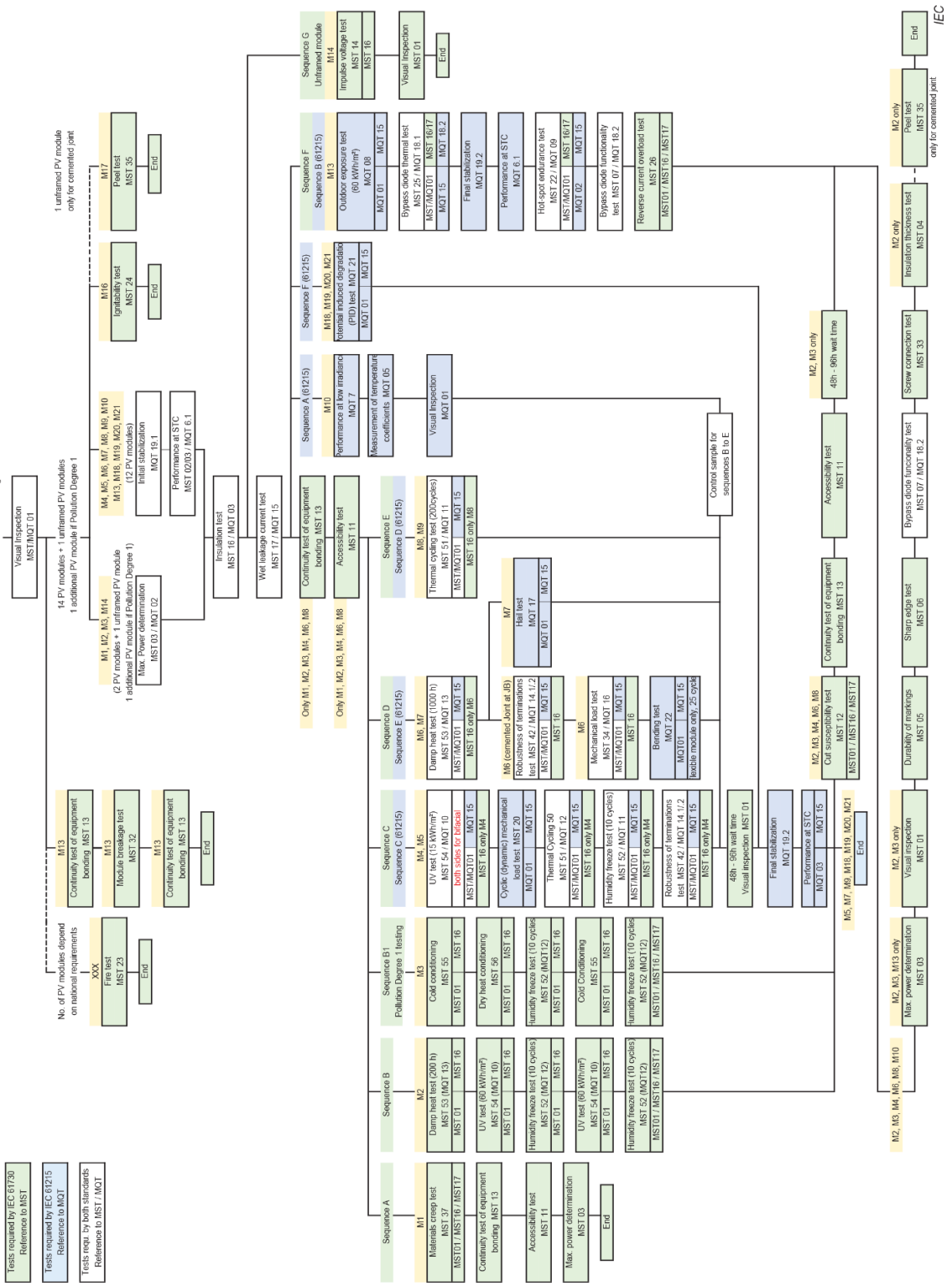


Figure 62: Combined test flow IEC 61215 and IEC 61730; from: Rettest Guideline IEC TS 62915, Ed. 2.0, 2023-09

| Deliverable 3.5 | TEST | MODULE SIZE | # MODULES | WHEN |
|---|---|---|---|---|
| Gen-0 GG M2 mono | Outdoor | 60 cell | 2 | M12 |
| | PTC | 16 cell | 1 | |
| | DH | 16 cell | 1 | |
| Gen-0 GG M2 bifi | Outdoor | 60 cell | 2 | M12 |
| | PTC | 16 cell | 1 | |
| | DH | 16 cell | 1 | |
| Gen-1 GG HM6 mono | PTC | 120 half-cells | 2 | M21 |
| | DH | 120 half-cells | 2 | |
| | HF | 32 half-cells | 2 | |
| | Mech. load | 120 half-cells | 1 | |
| | Outdoor | 120 half-cells | 12 | M23 |
| Gen-1 GG HM6 bifi | PTC | 120 half-cells | 2 | M22 |
| | DH | 120 half-cells | 2 | |
| | HF | 32 half-cells | 2 | |
| | Mech. load | 120 half-cells | 1 | |
| | Outdoor | 120 half-cells | 4 | M23 |
| Low CTM losses record modules special modules | demonstrator | 120 half-cells | 12 | M12 until M36 |
| Certification (Gen-1 GG HM6 mono) | VDE or TÜV | 120 half-cells | 20 | M27 |
| Sum 60(120)-cell | | | 62 | |
| Sum 16(32)-cell | | | 8 | |

Table 8: Details of Deliverable 3.5

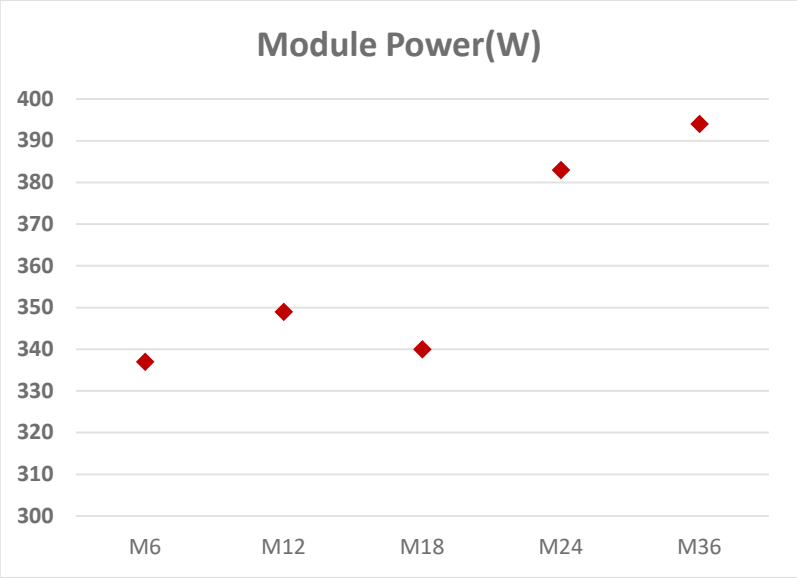


Figure 63: Power increase with successive IBC Module demonstrators during the three years of the project, starting from M2 & HM2 (blue) ending to HM6 (red) solar cells.

## 2.3 Module installation and outdoor monitoring (WP4)

### 2.3.1 Module installation (MBR, M12-M24) (Task 4.1)

During the first project year we have selected the leading high performance module available on the Swiss market and purchased those modules through official trade channels. The selected modules where then tested internally with a high precision module measurement at PASAN that allowed to measure all modules under comparable conditions calibrated to our internal IBC cell measurement using a laminated IBC single-cell module. However, there was no spectral mismatch correction carried out for the module measurement, which is generally also not applied to standard module measurements, partly due to the calibration standards used being of the same cell technology as used for the module, thus the mismatch factor is negligible.

| Manufacturer | Sunpower | | LG | REC | Meyer Burger | | | |
|---|---|---|---|---|---|---|---|---|
| model | SPR-MAX3-430 | SPR-MAX5-410-AC | 400Q1C | alpha | half white M6 | half black M6 | half GG front | bifi M6 |
| Power [W] data sheet | 430 | 410 | 400 | 355 | "375" | "365" | "380" | |
| Power [W] measurement | 420.3 | 408.0 | 404.6 | 355.6 | 378.4 | 374.2 | 378.4 | |

Table 9: added commercial best in class modules

With SunPower and LG we acquired 2 IBC technology modules that are similar to MBR's IBC in terms of cell contacts (all on the rear side) but different in cell technology, i.e. high temperature cell processing (in case of LG and SunPower) vs. low temperature heterojunction based technology in case of the IBC in the Sirius project. The modules from REC and Meyer Burger are of heterojunction technology (HJT)

with traditional front and rear side contacts. The modules in the table were very early production modules received from the MB factory in Freiberg, Germany. The data sheet specification for those modules were still not released thus the values are given in quote-marks. For the bifacial module, we also measured the bifaciality and the typical rated power for a bifacial performance measurement, i.e. an additional 200W/m$^2$ from the rear side, which brings the bifacial module to around 447 W.

Following modules measurements the above listed new modules were installed on spare slots on MBR's roof monitoring facility established in the preceding SFOE supported SwissInno HJT project. Added to this installation were the first prototype modules with the new IBC technology mentioned above (Gen0 & Gen1). The monitoring power electronics needed to be upgraded to the state-of-the-art module powers that in the meanwhile have advanced beyond 400 W, mostly due to larger module sizes but also due to increased cell efficiencies in recent years.

Figure 64: Photo of MBR's outdoor monitoring facility with some of the modules mentioned in the text above.

Since the beginning of 2022 the yield of all the above mentioned and several more modules is monitored. We already started preliminary analysis of module yields and are currently improving and progressing our methods to understand the performance of the new technology in detail and establish a good and meaningful comparison to the other monitored technologies.

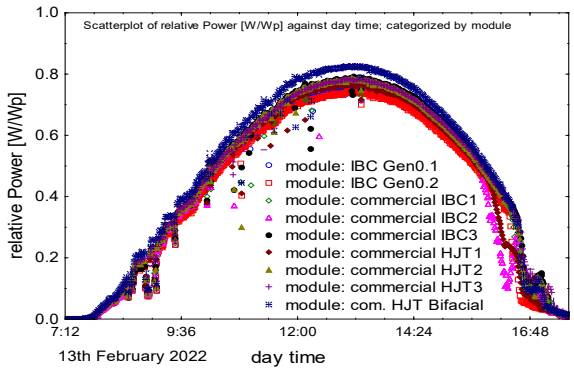


Figure 65: Example for the yield monitoring of various modules power generation profile during the 13$^{th}$ of February 2022. The bifacial HJT module exceeds the other modules in this data presentation, because the power is normalised to the conventional module rating (i.e. monofacial measurement)

Unfortunately, an unanticipated event (Innoparc roof refurbishing) imposed to remove the whole monitoring installation from the SIRIUS project, when the latest HM6 IBC modules were manufactured. A solution was found thanks to the EPFL monitoring system, which was able to receive two IBC modules produced during the SIRIUS project. A picture of the installation is presented below:

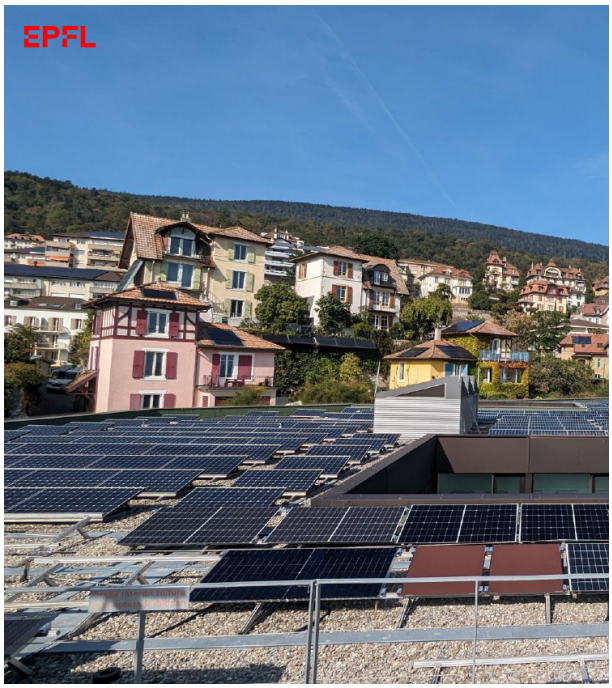


Figure 66: EPFL Monitoring Installation

Thanks to this backup solution, 2 generations of IBC modules (Gen1 and Gen2) were monitored and presented below. The energy yield of the latest IBC module (Gen 2), outperforms the first generation and notably overpasses the standard 395W HJT white module from Meyer Burger production. This encouraging results allows to anticipate an even better performance when the technology will be mass produced, as non-uniformity from the different remaining manual handling stations (cell and module) were preventing to fully exploit the tunnel IBC technology.

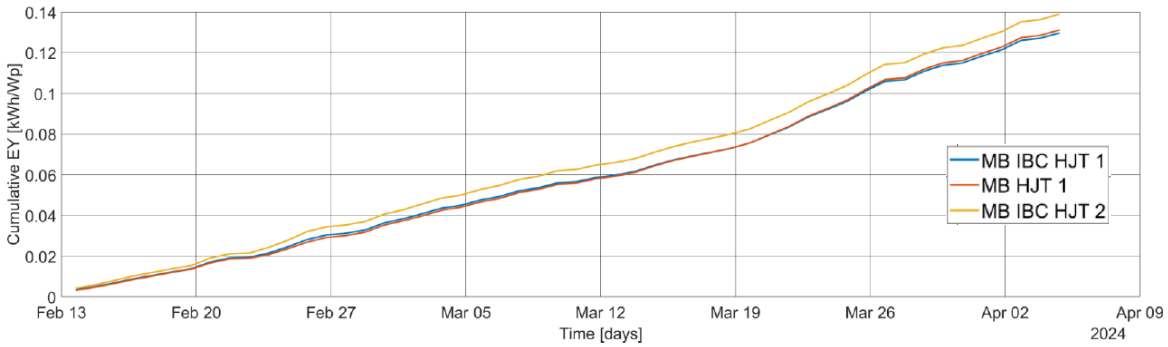


Figure 67: Cumulative Energy Yield (Kwh/Kwp) for the 2 IBC HM6 modules (Gen1 and Gen2) in comparison to the HJT module.

To better understand the module power potential (or performance limitations) for our tunnel IBC technology and also the other monitored technologies from 3rd parties, we applied a key metric of cell performance monitoring we developed within and for this project that calculates the uniformity of the EL signal across the cell and correlates it to the cell's total FF. With this metric we find a strong correlation between a uniform EL signal across a cell and its FF or maximum power point.

The application for the metric and performance limitation concept on modules yielded the correlation depicted in Figure 68. The measure of 'non-uniformity of the EL signal is calculated from the ratio of the signal standard deviation to the signal average.

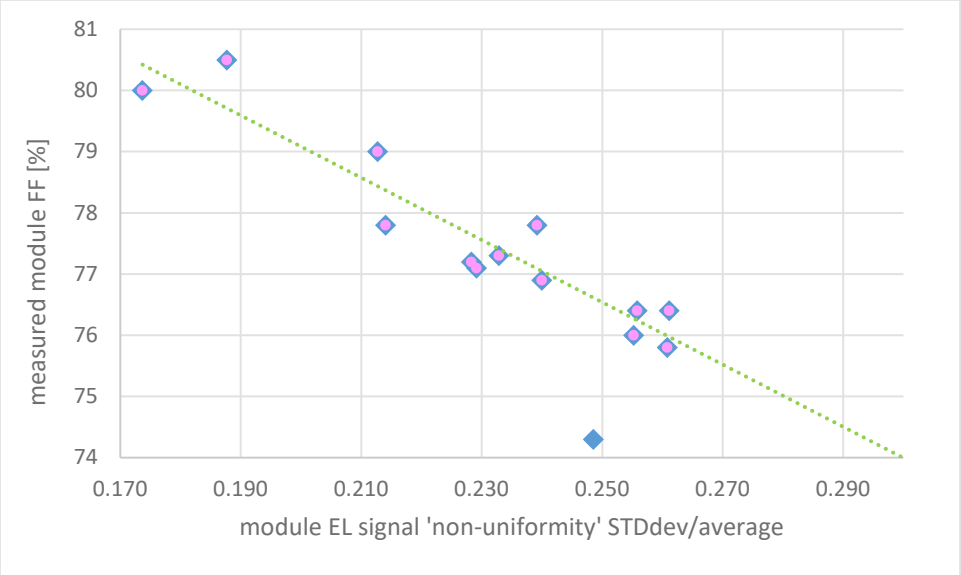


Figure 68: Measured FF of 12 ICB modules from this project with some additional modules from other manufacturers versus the measure of 'non-uniformity' of the EL signal of the entire module.

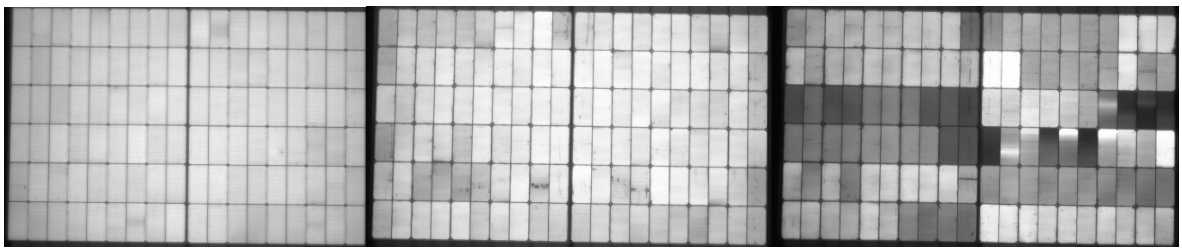

Figure 69: Examples of module EL images, left quite uniform EL image from 3rd party module, middle best performing module in the project, right module with a high 'non-uniformity'.

From the metric and performance analysis we can conclude that uniformity between all the cells in the module and the uniformity of each individual cell in the module is a major enabler for high module performance and power. Thus, we also understand the performances and the limitations of all the modules manufactured in the project. Due to limited cell production capabilities the project modules could not be made from the same tight binning as can be done in mass production. Now understanding the limitations given by the uniformity, we can gauge the potential for our modules in production through the assumption that a better uniformity distribution in the module can be achieved with tighter binning from a production. The module power potential of the current IBC technology would be between 402 Wp to 407 Wp assuming a similar good uniformity as measured for industrially produced modules. This is

around 10Wp higher than the best module measured in the project and this would also fulfil the project objective to demonstrate a module power of equal or greater 400 Wp.

With the new monitoring capability at EPLF/CSEM we started to collect more outdoor data in 2024 that enables us to analysis the outdoor performance of the tunnel IBC technology and compare it to the HJ Technology or IBC products from manufacturers that use other IBC technologies. In general it needs to be mentioned that outdoor data are more demanding to analysis since it needs a lot experience to select the proper conditions for comparison and to separate various effects that are influencing measurement data all at the same time, like temperature, irradiance, influence of surrounding, and even shading elements. Additionally, the measurement data might carry higher uncertainties than well calibrated indoor measurements.

As an example for the performance ratio of the different monitored modules we select a clear day in February 2024 with a peak irradiation measured at ~600 W/m2 as is shown in Figure 70. We see that depending on the roof position the modules are not receiving the same irradiance in the morning due to the flat angle of the sun irradiation in February. If we just analyse the data from 12:30h up to around 16h, we see the lower normalised power for the Gen1 IBC module (MB IBC HJT 1) and the MB HJT module, followed by the HJT HUASUN and REC modules. Quite similar in normalised power are the IBC modules from Longi, Sunpower and rather encouragingly the 'improved' Gen2 IBC module (MB IBC HJT 2, dark red dots). The Gen2 IBC R&D module has between 5% - 7% higher normalised power compare to the industrial Meyer Burger HJT module and is basically on par with the high performing commercial IBC modules.

The reason for the better performance of the Gen2 IBC module is quite likely linked to the thermal behaviour of the module. When evaluating the median temperature of the modules as a function of irradiance that heats the modules up we can establish and compare the operation temperature as can be seen in Figure 71.

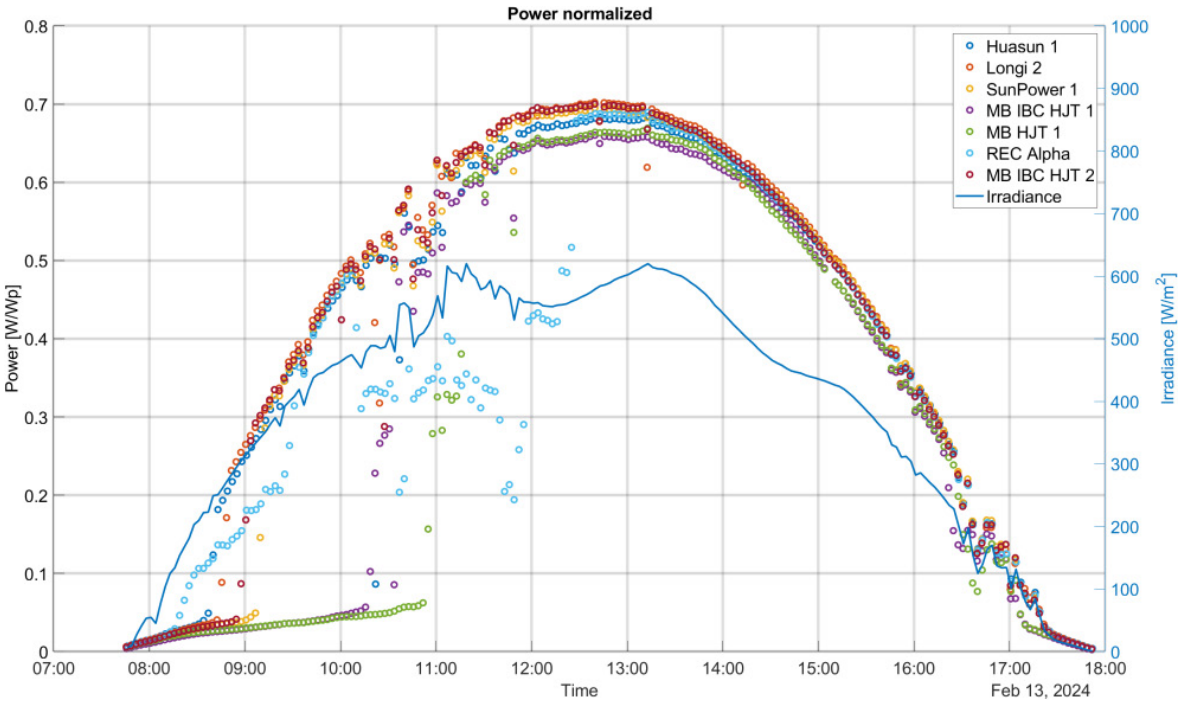


Figure 70: Normalized module power in [W/Wp] for the modules monitored in the project measured on 13.02.2024. The measured irradiance of up to 600W/m2 at around 13 o'clock is also displayed with the units on the right axis.

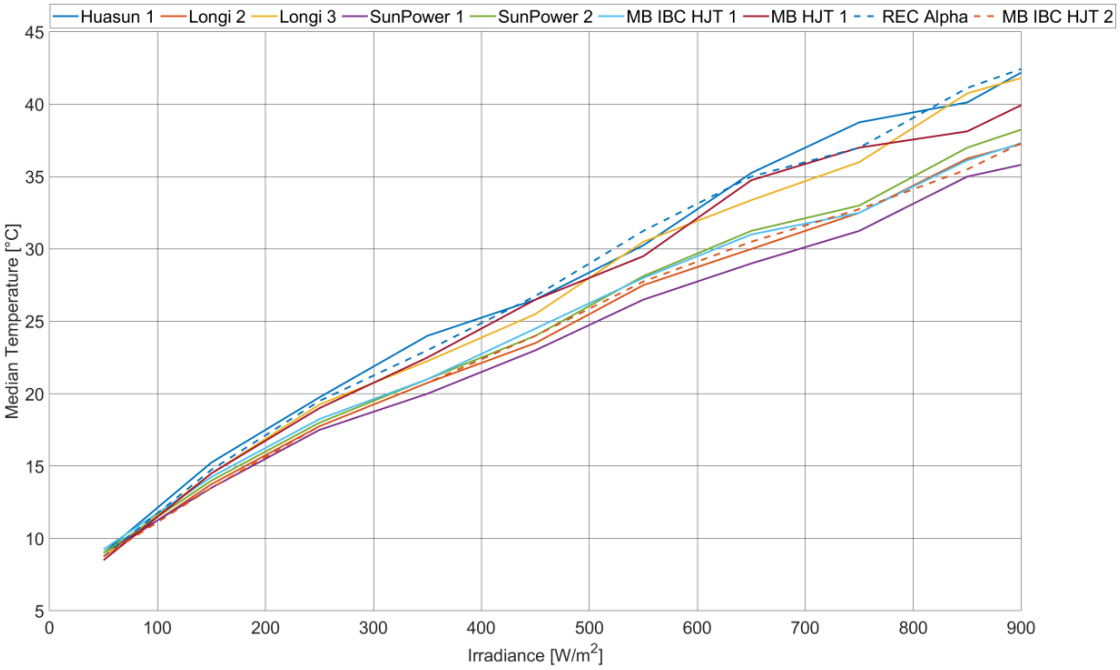


Figure 71: Median module temperature displayed over the incident irradiation that heated up the modules. 2 groups can be distinguished, one that heats up more with most of the HJT modules and one that stays a bit cooler with all the IBC modules.

The lower operation temperature measured for the IBC modules explains some of their higher normalised power, however not all of it. In Figure 71 we have a module operation temperature difference of up to 6K between the coolest and the hottest module at around 600 W/m$^2$. We can estimate a performance difference with a high temperature coefficient of -0.3%/K of around 2 % between the coolest and the hottest module. This 2 % are roughly 1/3 of the observed difference in normalised power measured on the 13.02.2024 as shown in Figure 70. Or more precisely, it explains practically the difference of the IBC modules to the REC and HUASAN module, however, not to the MB HJT 1 and MB IBC HJT 1 modules.

As we observe already quite encouraging performances for the Gen2 IBC module we keep on monitoring and refining data analysis through 2024 which will produce a more complete picture with larger variations in irradiance and temperature still to come.

## 2.4 Model for the estimation of cost of owner ship (CoO) and levelized cost of energy (LCOE) related to the tunnel-IBC technology (WP5)

### 2.4.1 CoO-model

The CoO (Cost of Owner ship) being by definition a sensitive information, only a relative comparison will be mentioned based on the known HJT technology produced by Meyer Burger. The main characteristics of the Tunnel IBC technology developed during the Sirius project against the Heterojunction technology are summarized below at cell and module level:

Tunnel-IBC Cell:

- No Indium
- Silver content is strongly reduced
- More equipment are needed for PECVD, PVD layers deposition.

Tunnel-IBC Module:

- Single foil on rear (instead of 2 foils – front and rear for HJT)
- Less SWCT due to optimized electrode design
- Thinner encapsulant on front side thanks to the absence of wires.

The M6 wafer size being already phasing out in the industry, the comparison has been estimated based on the standard mainstream M10 wafer size and a 108-half cells module layout. All the material consumption achieved and presented in WP2 and WP3 has been scaled to this wafer area for the cost calculation. Figure 72 represents the estimated cost difference between IBC and HJT. The estimation takes into account the configuration difference of both manufacturing lines, impacting the total equipment cost, the yield and the operational cost (OPEX).

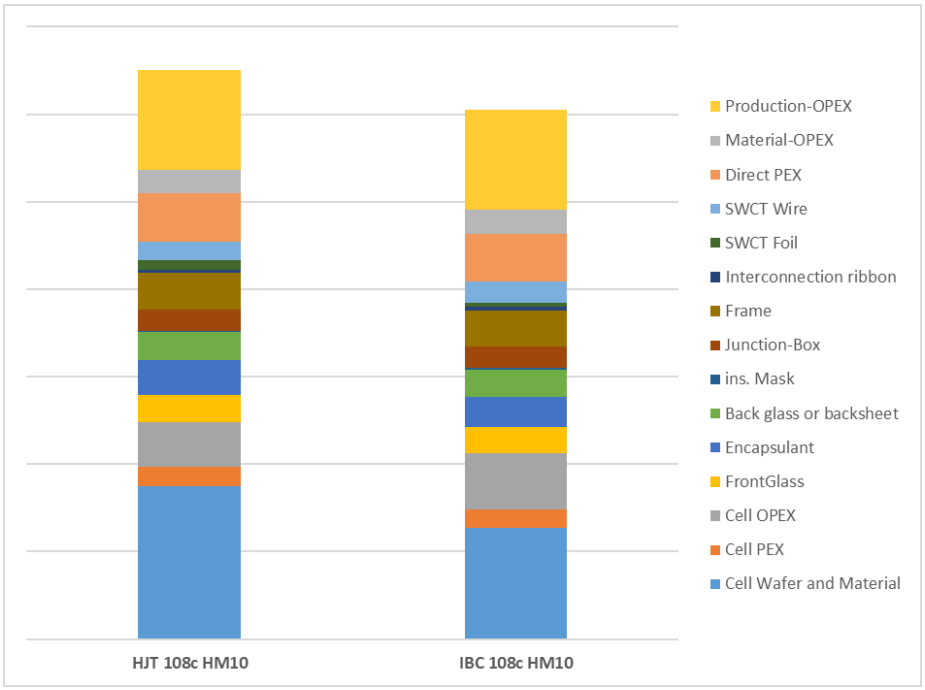


Figure 72: Cost comparison (A.U.) of both HJT and tunnel IBC technologies

All in one, the cost of the tunnel IBC module is estimated to be 7% lower compared to the HJT module. This cost reduction is mainly due to the strong R&D effort put during Sirius on metallization side, encapsulants and optimum Smart Wire Connection Technology optimisation which enable to compensate for the added machines into the cell line. Translating in €($)/Wp, the difference increases to 12% thanks to the expected higher power of the IBC module (450W) versus (430W) for the HJT technology.

### 2.4.2 LCOE model

The LCOE (Levelized Cost of Electricity) simulation is an important factor to estimate the bankability of the PV technology. It involves all parameters allowing to define the energy output of the installation and all financial related topics. As a reminder the basic LCOE model is defined as:

$$LCOE\left(\frac{CHF}{Kwh}\right) = \frac{\sum_0^n Lifecyclecost}{\sum_0^n EnergyProduction}$$

Here, the cost of working capital has been omitted for simplicity, to reflect only the impact of the PV technology and its parameters on the LCOE. The *Total life cycle cost* reflects the total investment of the PV installation (including inverter, installation cost, administration etc.…) including the operation and maintenance costs over the installation lifetime. The *Total lifetime Energy production* reflects the total energy produced by the PV system over its lifetime until failure, including its 1st year degradation and the following degradation rate.

From the results of the Sirius project, we can highlight already three main factors which will benefit to a positive LCOE results thanks to:

- A demonstrated excellent reliability both at mini module level (up to 7-8x IEC norm) and full module size (4x IEC norm). This allow estimating lifetime from 30 years to potentially 40years, 25 years being the current reference value for mainstream technologies.
- A lower manufacturing cost (-12 %) as presented in the CoO above, which would translate directly into cheaper PV module therefore a reduced Total life Cycle cost.
- A better energy yield (+6%) as shown from the outdoor monitoring during ~3 months in 2024. These data cover intrinsically the temperature behaviour, the low light irradiance response, etc… and can be considered as more reliable than an extrapolation from indoor measurements.

In order to be closer to reality, the LCOE model is based on a real installer quotation from 2024 (i.e 33 kCHF without subsidies for 12.5 kW TopCon PV modules) in the case of a residential installation in Switzerland. The reference HJT module cost is estimated in this model to be similar to TopCon technologies nowadays.

The technical and financial parameters of the installation are presented in the table 10 below for both HJT and IBC technologies:

| | HJT | IBC |
|---|---|---|
| Module Power (W) | 430 | 450 |
| Module Lifetime (years) | 25 | 30 |
| Inverter lifetime (years) | 10 | 10 |
| Module Cost (unit) | 125 | 110 |
| Total Life cycle cost (CHF) | 34375 | 33940 |
| Initial degradation | 2% | 2% |
| Degradation rate (%/year) | 0.25 | 0.25 |
| Installation capacity (29 panels) kWp | 12.5 | 13 |
| Delta Energy yield IBC/HJT (%) | | 6% |
| Total lifetime energy production (kWh) | 339892.1 | 446730.8 |
| LCOE (CHF/kWh) | 0.101 | 0.075 |

Table 10: Inputs parameters for LCOE simulation

Even though the initial degradation rate and following degradation rate are kept the same for both technology in this first example, the higher module lifetime until failure considered (30 years, i.e. +20%), the higher energy yield (+6%) together with the initial higher performance (450W, +4.6%) reduce the electricity production cost by 25%, reaching 7.5ctsCHF/Kwh.

Others LCOE scenarios presented in Figure 73, such as a lower degradation rate (-0.1%) or a higher energy yield (+10%) do not impact significantly the final LCOE. In contrary, extending the module lifetime to 40years instead of 30years strongly reduces it, reaching 6.1ctsCHF/kWh. Interestingly, the module cost does not play a major role in the LCOE. In this example, despite a more expensive IBC module simulated (+40%), the LCOE rises only by 10%, i.e from 7.6ctsCHF/kWh to 8.6ctsCHF/kWh.

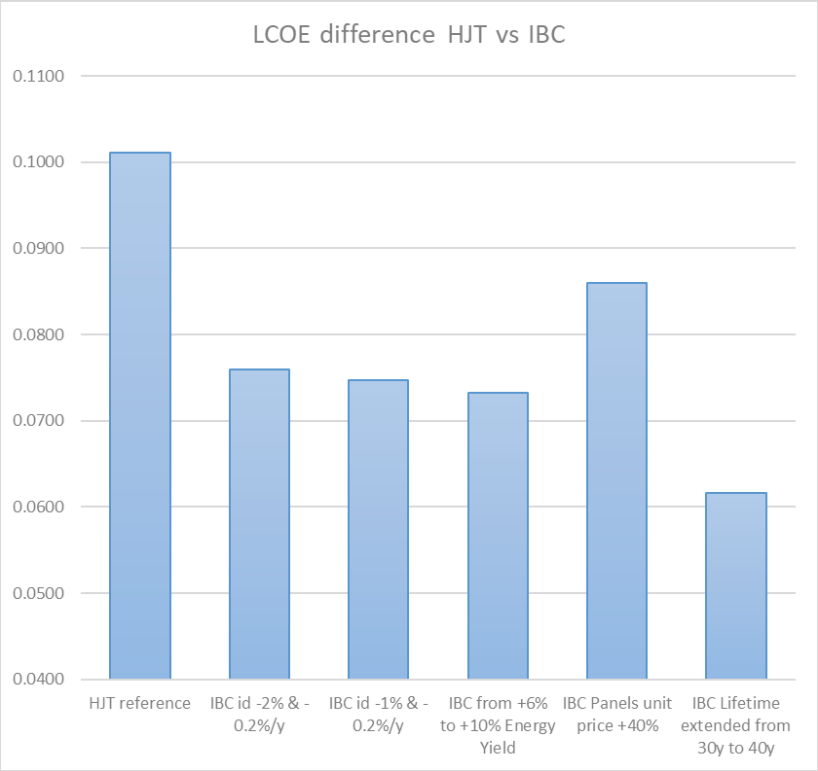


Figure 73: LCOE (CHF/kWh) of the HJT and IBC technologies, in the case of a residential installation in Switzerland.

As a consequence and to generate a wider discussion about the current debate about financial support about PV in Europe, the resilience bonus or others support policies discussed nowadays to restore the manufacturing of PV cells and modules would not dramatically increase the LCOE compared to modules made in China. In case of a residential PV installation, which still represent about ~50% of the European market, it would remain extremely competitive to install made in EU modules in comparison to the electricity from the grid (8-10cts for PV versus ~35ctsCHF/kWh for the grid in Switzerland in 2024).

In conclusion, module lifetime and (initial) Energy Yield are by far the two factors impacting the LCOE, before module cost or even degradation rate. Considering the outstanding reliability of IBC modules measured during the Sirius project, the LCOE would be in favor of the tunnel-IBC technology against alternatives mainstream modules (PERC, TopCon) even though its manufacturing cost would be higher in Europe.

## 2.5 Major outcome of Sirius after 3-years of project

After 3-years, the project has been globally successful with the highlights/lowlights listed below:

Highlights:

- Ultra low silver consumption achieved, making the tunnel-IBC technology competitive compared to the mainstream modules (TopCon, PERC). Manufacturing cost are expected to be lower than HJT thanks to silver and indium reduction and a less material consumption at module level.
- Outstanding reliability exceeding the IEC norm by far (between 4x to 5x with a maximum of 2% relative degradation)
- Good progress on half M6 cell efficiency up to 24.5%.

- CCS and RRU platforms fully operational to build IBC strings.
- Best 120x HM6 Module reached 394W based on 23.8% cells efficiency, confirming minimum CTM values about 0-1%.
- Outdoor Monitoring confirmed the benefit of the IBC in comparison to HJT technology with an energy yield gain of ~ 6%

Lowlights:

- Bifaciality processes requires more development and are now challenged cost wise (due to low silver consumption) by the mono-facial configuration developed during SIRIUS.
- Field monitoring will be delayed for Q3 2024, as the rooftop needs to be refurbished.
- Neither the 25.5% record cell nor the 400W module were achieved in due time and will require extra work but are achievable results with a fully automated production cell and module lines.

Notably, findings in Sirius triggered the submission of new patents, with a patent portfolio composed by seven submitted patents from which already four granted. A list of the patents portfolio is shown in the table below:

| Referenz | title | picture | Keyword | publ. No. |
|---|---|---|---|---|
| P20002 | Photovoltaic device and method for manufacturing the same |  | IBC HJT tunnel junction - a-Si shoulders | EP3770975A1 |
| P20004 | Photovoltaic device and method for manufacturing the same | 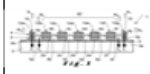 | Marks for IBC-Mask Alignment, IBC Fiducials | EP3886185A1 |
| P20006 | Photovoltaic device and method for manufacturing the same | 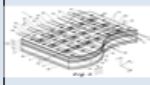 | IBC HJT with simplified process flow - "IBC mushroom" | EP4078683A1 |
| P20007 | Photovoltaic device and method for manufacturing the same | 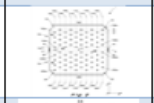 | IBC half cell smart manufacturing, IBC Flip-Flop | WO2023001509A1 |
| P20009 | Photovoltaic device and method for manufacturing the same | 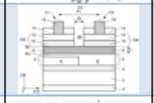 | MFL Multi-Functional-Layer | WO2024100249A1 |
| C10028 | Photovoltaic device and method for manufacturing the same |  | IBC tunnel-junction base patent | EP3371833A1 |
| C10030 | transparent patterning process for local insulation of back contacted silicon heterojunction solar cells and modules |  | Bi-facial IBC | EP3817070B1 |

Table 11: Current patents portfolio about the Tunnel-IBC technology.

# 3 Conclusion and Next steps

In conclusion, the Sirius project has enabled the upscaling of the tunnel IBC technology from 200cm$^2$ hand-made solar cells to full area industrial wafers and modules processed with new semi-automated tools. During the three years of the project, the new-patented rear electrode design successfully reduced the silver content down to 3mg/Wp, enabling significant manufacturing costs reduction in comparison to the existing heterojunction technology. The project has addressed a large landscape of objectives, from process challenges to automation new concepts and finally demonstrated the technology superiority of the tunnel IBC when it comes to outdoor monitoring, with a better energy yield comparable to the best IBC modules available on the market. A large part of the development focused on the reliability topic, with successful demonstrators passing easily the standard stress tests.

All these developments enable to launch the next steps, i.e. the development and manufacturing of high throughput machines for both cells and modules in the European PILATUS project. Both cell and module pilot line will be located respectively in Germany and Switzerland. These new manufacturing lines will process larger wafer format (M10) and the standard 108c layout for residential products and 144c layout for utility scale panels.

Besides the two pilot lines, the tunnel IBC technology will be further developed at Meyer Burger Research to integrate new characteristics at cell level. A bypass diode behaviour, enabling a better response to hot spot stress tests is under development and the bifacial process will be further optimized in order to open the tunnel IBC technology to the growing utility scale segment, either in US or in Europe, with module power exceeding 600W.

# 4 Communication

The SIRIUS project has been highlighted in several conferences:

- 04/11/2021, SwissConnect PV conference, Yverdons les bains.
- 29-30/03/2022, 13$^{th}$ PV-tagung, Bern, (Poster presentation). The SIRIUS project won the best poster award in the field “scientific/technic contribution”.
- 03/04.11.2022, 5$^{th}$ SHJ conference, Aix-les-bains, France: “GW-scale manufacturing at MB”.
- 21/22.11.2022, 10$^{th}$ BC workshop, Konstanz, Germany, “The Sirius project: Tunnel IBC solar cell and module upscaling at Meyer Burger Research”
- 08.03.2023, EPFL Engineering Industry Day, Lausanne, Switzerland, “From laboratory solar cells to the largest manufacturing of solar cells in Europe”.
- 21.03.2023, 14th PV-tagung, Bern, Switzerland, « Le projet P+D SIRIUS : développement de la technologie Tunnel IBC au stade pré-industriel »
- 14.04.2023, nPV conference, Delft, Netherlands, “Tunnel-IBC solar cells”.
- Bulletin.ch, (29.09.2023), Vers l’industrialisation des cellules tunnel-IBC - Bulletin FR
- Hanover, Germany, (28.11.2023), BC Workshop, « Tunnel IBC solar cells and modules»

# 5 Reference


[1] https://table.media/en/china/news/solarwatt-surrenders-to-chinese-competition/

[2] https://www.pv-magazine.com/2024/02/02/chinas-new-pv-installations-hit-216-88-gw-in-2023/

[3] https://global.chinadaily.com.cn/a/202402/29/WS65dfd921a31082fc043b9af9.html

[4] https://www.reuters.com/business/energy/solar-suppliers-call-eu-aid-imports-crush-margins-2024-03-21/

[5] Energy Environ. Sci., 2021, 14, 5587

[6] ITRPV 2023, Markus Fischer

[7] https://copperalliance.org/

[8] https://www.silverinstitute.org/

[9] https://www.statista.com/statistics/

[10] https://pubs.usgs.gov/periodicals/


Project HALBION: https://www.aramis.admin.ch/Default?DocumentID=68900